



HAL
open science

Lithium isotopes in large rivers reveal the cannibalistic nature of modern continental weathering and erosion

Mathieu Dellinger, Jérôme Gaillardet, Julien Bouchez, Damien Calmels, Valier Galy, Robert Hilton, Pascale Louvat, Christian France-Lanord

► To cite this version:

Mathieu Dellinger, Jérôme Gaillardet, Julien Bouchez, Damien Calmels, Valier Galy, et al.. Lithium isotopes in large rivers reveal the cannibalistic nature of modern continental weathering and erosion. *Earth and Planetary Science Letters*, 2014, 401, pp.359 - 372. 10.1016/j.epsl.2014.05.061 . hal-01767766

HAL Id: hal-01767766

<https://hal.univ-lorraine.fr/hal-01767766>

Submitted on 11 Sep 2020

HAL is a multi-disciplinary open access archive for the deposit and dissemination of scientific research documents, whether they are published or not. The documents may come from teaching and research institutions in France or abroad, or from public or private research centers.

L'archive ouverte pluridisciplinaire **HAL**, est destinée au dépôt et à la diffusion de documents scientifiques de niveau recherche, publiés ou non, émanant des établissements d'enseignement et de recherche français ou étrangers, des laboratoires publics ou privés.



Distributed under a Creative Commons Attribution - NonCommercial 4.0 International License

Durham Research Online

Deposited in DRO:

13 April 2015

Version of attached file:

Accepted Version

Peer-review status of attached file:

Peer-reviewed

Citation for published item:

Dellinger, M. and Gaillardet, J. and Bouchez, J. and Calmels, D. and Galy, V. and Hilton, R. G. and Louvat, P. and France-Lanord, C. (2014) 'Lithium isotopes in large rivers reveal the cannibalistic nature of modern continental weathering and erosion.', *Earth and planetary science letters.*, 401 . pp. 359-372.

Further information on publisher's website:

<http://dx.doi.org/10.1016/j.epsl.2014.05.061>

Publisher's copyright statement:

NOTICE: this is the author's version of a work that was accepted for publication in *Earth and Planetary Science Letters*. Changes resulting from the publishing process, such as peer review, editing, corrections, structural formatting, and other quality control mechanisms may not be reflected in this document. Changes may have been made to this work since it was submitted for publication. A definitive version was subsequently published in *Earth and Planetary Science Letters*, 401, 1 September 2014, 10.1016/j.epsl.2014.05.061.

Use policy

The full-text may be used and/or reproduced, and given to third parties in any format or medium, without prior permission or charge, for personal research or study, educational, or not-for-profit purposes provided that:

- a full bibliographic reference is made to the original source
- a [link](#) is made to the metadata record in DRO
- the full-text is not changed in any way

The full-text must not be sold in any format or medium without the formal permission of the copyright holders.

Please consult the [full DRO policy](#) for further details.

1 **Lithium isotopes in large rivers reveal the cannibalistic nature**
2 **of modern continental weathering and erosion**
3
4
5

6 Mathieu Dellinger^{a,b,*}, Jérôme Gaillardet^{a,c}, Julien Bouchez^{a,d},
7 Damien Calmels^e, Valier Galy^f, Robert G. Hilton^g, Pascale Louvat^a, Christian France-
8 Lanord^h
9

10
11
12 ^aLaboratoire de Géochimie et Cosmochimie, Institut de Physique du Globe de Paris
13 (IPGP), UMR 7154 CNRS, Université Paris Diderot, 1 rue Jussieu, 75238 Paris, France
14

15 ^bGEOTOP, Université du Québec à Montréal, Montréal, Québec H3C 3P8, Canada
16

17 ^c Institut universitaire de France
18

19 ^d GFZ German Research Centre for Geosciences, Telegrafenberg, 14473 Potsdam,
20 Germany.
21

22 ^e Laboratoire de Géochimie des Isotopes Stables, Institut de Physique du Globe de Paris
23 (IPGP), UMR 7154 CNRS, Université Paris Diderot, 1 rue Jussieu, 75238 Paris, France
24

25 ^f Woods Hole Oceanographic Institution, Department of Marine Chemistry and
26 Geochemistry, 360 Woods Hole Road, Woods Hole, Massachusetts 02543, USA.
27

28 ^g Department of Geography, Durham University, Science Laboratories, South Road,
29 Durham, DH1 3LE, UK.
30

31 ^h Centre de Recherches Pétrographiques et Géochimiques (CRPG-CNRS), 15 rue Notre
32 Dame des Pauvres, 54501 Vandoeuvre les Nancy, France.
33

34
35 *Corresponding authors, equal contribution authors:
36 dellinger@ipgp.fr
37
38
39
40
41

42 Keywords: Lithium isotopes, Chemical weathering, Sedimentary recycling, Large Rivers
43
44

45
46
47
48
49
50
51
52
53
54
55
56
57
58
59
60
61
62
63
64
65
66
67
68
69
70
71
72
73
74
75
76

Abstract

The erosion of major mountain ranges is thought to be largely cannibalistic, recycling sediments that were deposited in the ocean or on the continents prior to mountain uplift. Despite this recognition, it has not yet been possible to quantify the amount of recycled material that is presently transported by rivers to the ocean. Here, we have analyzed the Li content and isotope composition ($\delta^7\text{Li}$) of suspended sediments sampled along river depth profiles and bed sands in three of the largest Earth's river systems (Amazon, Mackenzie and Ganga-Brahmaputra rivers). The $\delta^7\text{Li}$ values of river-sediments transported by these rivers range from +5.3 to -3.6‰ and decrease with sediment grain size. We interpret these variations as reflecting a mixture of unweathered rock fragments (preferentially transported at depth in the coarse fraction) and present-day weathering products (preferentially transported at the surface in the finest fraction). Only the finest surface sediments contain the complementary reservoir of Li solubilized by water-rock interactions within the watersheds. Li isotopes also show that river sediments can be interpreted as a mixture between unweathered fragments of igneous and sedimentary rocks. A mass budget approach, based on Li isotopes, Li/Al and Na/Al ratio, solved by an inverse method allows us to estimate that, for the large rivers analyzed here, the part of solid weathering products formed by present-day weathering reactions and transported to the ocean do not exceed 35%. Li isotopes also show that the sediments transported by the Amazon, Mackenzie and Ganga-Brahmaputra river systems are mostly sourced from sedimentary rocks (> 60%) rather than igneous rocks. This study shows that Li isotopes in the river particulate load are a good proxy for quantifying both the erosional rock sources and the fingerprint of present-day weathering processes. Overall, Li isotopes in rivers sediments confirm the cannibalistic nature of erosion and weathering.

1. Introduction

When water interacts with rocks at the Earth's surface, chemical weathering reactions neutralize the atmospheric acidity and transform rocks into dissolved chemical species. Newly formed secondary phases (clay minerals, iron oxides) accumulate in soils or are eroded and conveyed by rivers to sedimentary basins. These chemical weathering reactions are of major importance for the Earth system. On geological timescales, they control the evolution of climate through the consumption of atmospheric carbon dioxide (Berner et al., 1983; Gaillardet et al., 1999b; Raymo et al., 1988; Walker et al., 1981),

85 shape the Earth's surface through chemical denudation and soil production (Heismath et
86 al., 1997) and modify the composition of the continental crust (Lee et al., 2008; Liu and
87 Rudnick, 2011; Rudnick, 1995). Geochemical mass budgets of river-borne material
88 (dissolved and particulate phases) show that rivers transport both "present-day
89 weathering products" (new solid materials formed during the residence of sediment in
90 river basins by present-day water-rock interactions) and carry "inherited weathering
91 products" derived from older sedimentary rocks, which have been subject to previous
92 weathering episodes (Bouchez et al., 2011a; Gaillardet et al., 1999a). Moreover, on the
93 basis of the Nd isotope record of shales, Veizer and Jansen (1979, 1985) suggested that
94 the Post-Archean sedimentary cycle is 90% cannibalistic (i.e. 90% of the sedimentary
95 rocks are formed by the recycling of ancient sedimentary rocks). Recycling of cation-
96 depleted sedimentary rocks may have impacted the long-term evolution of Earth's
97 atmosphere by reducing the capacity of the crust to neutralize atmospheric acidity
98 through time (Gaillardet et al., 1999a). To test these hypotheses, first we need to quantify
99 the relative importance of present-day vs. inherited weathering signatures in river
100 sediments. However, the amount of "new" versus "old" weathered material transported
101 by rivers to the ocean is poorly constrained.

102 Over the last decade, lithium (Li) isotopes have proven to be a powerful tracer of
103 silicate weathering because: (i) Li is mobile (i.e. is mostly solubilized from minerals)
104 during water-rock interactions, (ii) Li is mainly derived from the chemical weathering of
105 silicate rocks (Kisakurek et al., 2005; Millot et al., 2010) while not involved in biological
106 processes (Lemarchand et al., 2010) and, (iii), Li isotopes are fractionated during
107 chemical weathering (Huh et al., 1998; Pistiner and Henderson, 2003), with preferential

108 incorporation of ^6Li in solid weathering products leaving the dissolved fraction enriched
109 in ^7Li . To date, measurements of Li isotopes on solid weathering materials have focused
110 on soil systems (Kisakürek et al., 2004; Lemarchand et al., 2010; Pogge von Strandmann
111 et al., 2012; Rudnick et al., 2004) or small rivers (Kisakurek et al., 2005; Kisakürek et al.,
112 2004; Vigier et al., 2009; Pogge von Strandmann et al., 2010; Wimpenny et al., 2010).
113 Here we extend the use of Li isotopes to sediments carried in large rivers, using depth-
114 profiles to sample the full range of solid products of weathering and erosion. Li isotopes
115 are used alongside element ratios which track sediment grain size, provenance and
116 chemical weathering processes (e.g. Al/Si, Na/Al, Li/Al) to construct a mass balance
117 model, allowing us to quantify the proportion of materials derived from present-day
118 chemical weathering, versus those inherited from previous weathering episodes. These
119 findings shed new light on the cannibalistic nature of Earth's erosion and weathering
120 engine and we discuss the possible implications for the drawdown of CO_2 by silicate
121 weathering.

122

123 **2. Geographical setting**

124

125 Large rivers integrate weathering and erosion processes over vast portions of the
126 continental crust and therefore provide insight on the major processes operating at Earth's
127 surface. In this paper, we investigated the erosion products transported in three large river
128 systems representative of various geodynamic settings (Fig. 1): the Amazon, Mackenzie
129 and Ganga-Brahmaputra river systems. These rivers together contribute to 10-15% of the
130 global suspended sediment flux to the ocean (Milliman and Farnsworth, 2011), and drain
131 various lithologies. The selected basins are characterized by moderate to high erosion
132 rates and so we do not consider lower erosion and weathering rate areas (e.g. Congo

133 River), nor volcanic islands. The results are likely to be representative of large
134 continental rivers draining “weathering-limited” areas and vast foreland basins, underlain
135 by mixed lithologies.

136

137 The Amazon River is the largest river system on Earth with a mean discharge of 209,000
138 m³/s and a suspended sediment flux of about 1000 Mt/yr (Wittmann et al., 2011b), with
139 the Andean cordillera (11% of the total Amazon river surface, altitudes ranging from 400
140 m to 6700 m) being the major sediment source area (Gibbs, 1967). We focus on the two
141 major tributaries which dominate the suspended sediment flux of the Amazon River’s:
142 the Solimões River (55% of the total long-term denudation flux) in the western part of the
143 basin and the Madeira River in the south (45% of the total denudation flux) (Wittmann et
144 al., 2011b). The Andean part of the Madeira River is almost exclusively composed of
145 uplifted Paleozoic to Tertiary sedimentary rocks while there is a significant proportion of
146 arc-type igneous rocks (mainly andesite) in the Andean part of the Solimões River basin.
147 In addition and to test the influence of lithology, we report data on the Beni River
148 (tributary of the Madeira River) which drains almost exclusively sedimentary rocks, and
149 on the Ucayali, Pastaza and Napo Rivers (tributaries of the Solimões) which drain a
150 significant proportion of igneous rocks.

151 The Mackenzie River basin is located in northwest Canada between latitudes 52°N and
152 68°N. It drains to the Arctic Ocean with a mean discharge of 9,700 m³/s and a mean
153 depth-integrated sedimentary flux of 124 Mt/yr (Carson et al., 1998). Aside being one of
154 the largest river basin in the world, the Mackenzie River has characteristics of interest
155 here because i) it is localized in the cold sub-Arctic to Arctic region with very low

156 chemical weathering rates, ii) about 70% of its basin rocks are covered by sedimentary
157 rocks, which combined with the low degree of chemical weathering, makes this basin
158 ideal to study recycling of sedimentary rocks iii) it drains a relatively pristine area.
159 Details about geology, climate and weathering rates can be found in the following studies
160 (Millot et al., 2003; Millot et al., 2010; Tipper et al., 2012). We sampled the Mackenzie
161 River immediately upstream of its delta in addition to the major tributaries in the basin:
162 the Peace-Slave River system in the southern part of the Mackenzie basin, the Liard, the
163 Peel and Red Arctic rivers in the northern part.

164 The Ganga-Brahmaputra (G-B) river system drains the Himalaya and is characterized by
165 high erosion rates with a mean suspended sediment flux of about 1000-2000 Mt/yr (Galy
166 and France-Lanord, 2001). The major Himalayan geological formations are from north to
167 south the Tethyan Sedimentary Series (TSS) composed by low-grade marine sedimentary
168 rocks; the High Himalayan Crystalline (HHC) composed of high-grade metasedimentary
169 rocks (amphibolite to granulite facies) with minor local leucogranite intrusions; the
170 Lesser Himalaya (LH) formed mostly by low-grade sedimentary rocks, and finally the
171 Siwaliks plain which correspond to Neogene deposits uplifted by the Himalayan
172 deformation front (Galy and France-Lanord, 1999, 2001; Lupker et al., 2012). Based on
173 Sr and Nd isotope ratios, about 80% of the river sediments are thought to be derived from
174 the HHC and 20% from the LH (Galy and France-Lanord, 2001). The Ganga and
175 Brahmaputra rivers were sampled at their outlet in Bangladesh (Lupker et al, 2011,
176 2012).

177

178 **3. Sampling strategy and analytical protocols**

179 Weathering and erosion produce solid particles with variable grain size, mineralogy and
180 weathering intensity. Sediments are naturally sorted within large rivers, with the finest
181 particles transported at the surface and the coarsest at the bottom of the channel. A novel
182 depth profile sampling approach was used herein order to take into account the variability
183 of the suspended sediment concentration, grain size and geochemistry across the whole
184 water column. This procedure has been presented and extensively discussed elsewhere
185 (Bouchez et al., 2011b; Galy et al., 2007; Lupker et al., 2011). Briefly, suspended
186 sediment samples were collected at discrete depths along vertical profiles using a 7 liters-
187 sampler similar to a horizontal Niskin type bottle. Profile sampling locations were chosen
188 based on ADCP (Acoustic Doppler Current Profiler) survey along river transects prior to
189 collection. ADCP quantifies flow velocity, river depth and cross section, water discharge,
190 and heterogeneity of river turbidity. River samples were transferred into sterilized plastic
191 bags of known weight. The sample set was completed by river sands collected from the
192 channel thalweg (using a bucket dredge) and from recent flood deposits on river banks. In
193 some cases, when depth-sampling was not possible, only surface suspended sediments
194 and bed sands were collected.

195 Using this sampling protocol, major tributaries and the mainstream of the Mackenzie
196 River were sampled during 3 consecutive years at different times over the hydrological
197 cycle, including at high water stage (July 2009, September 2010 and June 2011) to
198 capture the temporal variability of sediment transport. The Amazon River and tributaries
199 were sampled at various depths during several field campaigns between 2005 and 2008
200 (Bouchez et al., 2011a; Bouchez et al., 2012; Bouchez et al., 2011b). Surface samples
201 from the Beni River watershed were sampled in 2001 and 2007 (Dosseto et al., 2006,

202 Bouchez et al., 2012). Napo River samples are river bed sediments samples, sieved at 125
203 μm and provided by the German Research Centre for Geosciences (GFZ Potsdam)
204 (Wittmann et al., 2011a). Finally, the Ganga and Brahmaputra rivers samples from this
205 study are from field campaigns performed in 2008 by the “Centre de Recherches
206 Pétrographiques et Géochimiques” (Lupker et al., 2012) and from a field campaign
207 carried out in 1999 by IPGP (only surface and bed sediments samples) (Gaillardet et al.,
208 1999b).

209 River samples were filtered on-site using a frontal filtration system through 0.22 μm
210 porosity polysulfone 142 mm-membranes. Special attention was paid to recover all grain
211 sizes including the silt fraction that tended to settle in the sampling bags and the finest
212 particles that tended to sorb on the plastic wall. Sediments were recovered from the filters
213 and placed with filtered water in 125 ml-glass bottles. In the lab, river sediment samples
214 were dried either at 50°C or by freeze drying within 3 weeks of collection, crushed in an
215 agate mortar and their major and trace elements content were measured respectively by
216 ICP-AES and ICP-MS by the SARM (Service d’Analyse des Roches et des Minéraux,
217 INSU facility, Vandoeuvre-les-Nancy, France, analytical details available on
218 <http://helium.crgp.cnrs-nancy.fr/SARM>). Most of the Li concentration measurements (n =
219 119) were made by ICP-AES by the SARM with an analytical uncertainty of 5%. The Li
220 content of the remaining samples (n = 33) were measured by ICP-AES at the Laboratory
221 of “Géochimie des eaux” (IPGP, Paris) with an analytical uncertainty of 8%.

222 Before Li isotope analyses, Li was separated from the matrix by ion-exchange
223 chromatography using a method similar to James and Palmer (2000) after sample
224 digestion. A sample aliquot was loaded onto a column filled with 2.7 mL of AG50-X12

225 resin and the Li was eluted in HCl 0.2N. The 1 mL elution cuts immediately before and
226 after the elution peaks were collected in several occasions to check for absence of Li. At
227 least two Standard Reference Materials (BHVO-2, JB2, NASS-5, BCR-2) and one blank
228 were systematically processed in each chemistry session to control the reliability of the
229 separation. After the separation, the elution fraction containing Li (about 24 mL) was
230 evaporated at a temperature of about 90°C and kept as a solid salt until the measurement
231 session. Li isotope composition was measured using a MC-ICP-MS Neptune (Thermo
232 Scientific, Bremen) at IPGP using an APEX desolvation system and at typical Li
233 concentrations of 20-30 ppb. Each sample was successively measured 3 times within a
234 standard-sample bracketing (SSB) sequence, yielding five $\delta^7\text{Li}$ values, from which an
235 average value was derived. For each sample and bracketing standard, $^7\text{Li}/^6\text{Li}$ ratios were
236 recorded for 12 cycles of 8 seconds each, with typical signals of 0.4 V/ppb. Background
237 intensities were recorded before each bracketing standard and each sample, and corrected
238 for. The intensity of the background was no more than 0.5-1% of the sample intensity.
239 The uptake time was 90 sec and the wash-time 4 min, resulting in a throughput rate of
240 about 50 min/sample. The overall internal standard error of $^7\text{Li}/^6\text{Li}$ measurements of
241 samples was typically between 0.05 and 0.15‰ ($\pm 2\sigma$). The long-term reproducibility of
242 the measurement itself was checked by repeated measurements of the IRMM-016 ($\delta^7\text{Li} =$
243 $+0.14 \pm 0.24\text{‰}$, $\pm 2\sigma$, $n = 78$), and Li-SPEC ($\delta^7\text{Li} = +94.38 \pm 0.27\text{‰}$, $\pm 2\sigma$, $n = 69$). The
244 overall reproducibility and accuracy of the procedure (including solid sample digestion
245 and Li separation) was checked by repeated measurement of the basalt reference
246 materials JB-2 ($\delta^7\text{Li} = +4.47 \pm 0.53\text{‰}$, $\pm 2\sigma$, $n = 30$ separations and 15 digestions) and
247 BHVO-2 ($\delta^7\text{Li} = +4.34 \pm 0.41\text{‰}$, $\pm 2\sigma$, $n = 6$ digestions). In addition, several samples

248 were duplicated or triplicated, and for each sample we report the mean value of all the
249 duplicates. The duplicates standard error ($\pm 2\sigma$) was better than 0.5%. Finally, the
250 concentration of the total procedural blank (acid digestion and column chemistry) was
251 assessed to be less than 0.05 ng, i.e. insignificant compared to the amount of Li from the
252 samples.

253

254 **4. Results**

255 A wide range of Li isotopic composition is observed in sediments from large rivers
256 (Tables 1 to 3). Sediment depth-profiles show that some of the large river systems
257 investigated appear strongly stratified for Li-isotope and Li concentrations while some
258 others show no variation with depth (Fig. 2). The $\delta^7\text{Li}$ of analyzed Suspended Particulate
259 Matter (SPM) ranges from over -3.6‰ for surface sediments to $+1.5\text{‰}$ for bottom SPM
260 with significant overlap between the Amazon, Mackenzie and G-B river systems. In
261 general, fine surface SPM samples have low $\delta^7\text{Li}$ values while coarse SPM from the
262 bottom of the river profile have a higher $\delta^7\text{Li}$ signature (Fig. 3). River Bed Sands (RBS)
263 have systematically higher $\delta^7\text{Li}$ values compared to SPM, ranging between -2.0‰ and
264 $+5.3\text{‰}$ and thus confirm previous observations from small rivers (Kisakurek et al., 2005;
265 Pogge von Strandmann et al., 2010). Considering both SPM and RBS, we found similar
266 $\delta^7\text{Li}$ and Li concentration ranges within a single depth-profile and across the overall
267 dataset. Each river sediment depth profile defines a hyperbolic relation between the $\delta^7\text{Li}$
268 and the Al/Si ratio (Fig. 3). The Al/Si ratio is a grain size proxy (Bouchez et al., 2011a;
269 Lupker et al., 2011), and the trend suggests that any river sediment sample taken on a
270 river depth-profile can be described as a mixture between fine surface particle and coarse

271 bottom sediment components.
272 Using the depth-integrated values for the Amazon, Mackenzie, Ganga, Brahmaputra
273 rivers and surface sediments of the Orinoco (Huh et al., 2001) and Changjiang rivers
274 (Wang et al., 2008), we calculate a mean Li concentration and $\delta^7\text{Li}$ value for large rivers
275 sediments discharged to the ocean of 50 ± 15 ppm and $-1.5\pm 1\%$. This Li isotopic
276 composition of large river sediments is slightly lower but close to the mean composition
277 of the Upper Continental Crust ($0\pm 2\%$) of Teng et al. (2004) but significantly lower than
278 the mean value of global riverine dissolved load (Huh et al., 1998; Liu and Rudnick,
279 2011) calculated at $\delta^7\text{Li} = +23\%$. The results of this study confirm at the global scale that
280 weathering and erosion processes fractionate Li isotopes, with the heavy isotope being
281 concentrated in the dissolved load. They show that the Li isotopic shift between
282 suspended sediments and dissolved load in rivers is close to 24-25%.

283

284 **5. Discussion**

285 The Li content and Li isotope composition in the large river sediments showed significant
286 variability between locations, and within individual river depth profiles. These changes
287 may reflect variability in sediment provenance and/or the redistribution of Li and its
288 isotopes during chemical weathering, either in the present day, or inherited from the
289 geological past. Herein, we seek to explain the variability in the Li isotope composition
290 of sediments carried by these major river systems, first by assessing the patterns in coarse
291 RBS, before interpreting the composition of SPM in the Amazon, Ganga-Brahmaputra
292 and Mackenzie river basins.

293 **5.1. Li isotope signature of river bed sands: the crustal diversity**

294 We first focus on identifying the nature of the coarse component using Na/Al and $\delta^7\text{Li}$ vs,
295 Li/Al mixing diagrams (Fig. 4). Normalization to Al allows us to correct Li concentration
296 in sediments for the dilution by quartz, carbonate or organic matter, by analogy to other
297 elements redistributed by chemical weathering processes (Bouchez et al., 2012). All RBS
298 samples plot along a negative trend, with G-B bed sediments lying slightly below the
299 overall trend. This negative relationship does not reflect progressive weathering of fresh
300 bedrock – which would lead to a positive trend as weathering tends to deplete sediment in
301 ^7Li – and rather reflects a mixture between two end-members of distinct chemical and
302 isotopic signatures. This mixing interpretation is supported by petrological observations
303 (Franzinelli and Potter, 1983; Potter, 1978), indicating that RBS contain mainly rock
304 fragments, quartz and heavy minerals. Because alkali elements are virtually absent from
305 quartz and heavy minerals (Bouchez et al., 2011a; Vital and Statterger, 2000), the Li and
306 Na budgets of RBS are mostly controlled by the nature of their lithic fragments, thus
307 reflecting the composition of the unweathered or poorly weathered bedrock material. The
308 bedrock end-member with high $\delta^7\text{Li}$ ($> +3.5\text{‰}$), high Na/Al (> 0.25) and low Li/Al ($<$
309 0.45×10^{-3}) falls in the range of mantle-derived igneous rocks (Magna et al., 2006;
310 Schuessler et al., 2009; Teng et al., 2009; Tomascak et al., 2008). The RBS samples from
311 the Solimões, Ucayali, Liard and Slave rivers plot close to this end-member, which is
312 consistent with the presence of igneous rocks in their sediment source areas (Andes and
313 Rocky Mountains).

314 The second bedrock end-member has a signature consistent with that of shales, with high
315 Li/Al ratio (up to 1.10^{-3}), lower $\delta^7\text{Li}$ (0 to -2‰) and low Na/Al ratio (Holland, 1984; Qiu
316 et al., 2011a; Qiu et al., 2009; Teng et al., 2004). Shales are fine-grained sedimentary

317 rocks, formed in the ocean by the deposition of particles derived from the erosion and
318 weathering of continental rocks. Shales are enriched in Li compared to igneous rocks, a
319 feature attributed by Holland (1984) to the scavenging of seawater Li onto clays. The
320 RBS of the Beni River plot close to this end-member, here again consistent with what is
321 known of this basin's geology. The RBS samples from the G-B lie slightly below the
322 trend defined by Amazon and Mackenzie RBS (Fig. 4). This may be the result of a large
323 erosional contribution from the high-grade meta-sedimentary rocks of the High Himalaya
324 Crystalline Series (Galy and France-Lanord, 2001). High-grade metamorphism of
325 sedimentary rocks results in a loss of Li without isotopic fractionation during dehydration
326 processes (Penniston-Dorland et al., 2012; Qiu et al., 2011b). Accordingly, the average
327 chemical composition of the continental crust eroded from a given basin should lie
328 between the three end-members (igneous, low and high-grade meta-sedimentary rocks) of
329 Fig. (4). The use of RBS to derive the composition of the bedrock here is similar to the
330 approach of Hilton et al. (2010) for sourcing organic matter in Taiwanese rivers. Overall,
331 the low $\delta^7\text{Li}$ values of some RBS samples clearly demonstrate the presence of a recycled
332 meta-sedimentary component in the continental crust. This is consistent with the
333 conclusions inferred from the major elements in large river denudation products
334 (Gaillardet et al., 1999a).

335 **5.2. Li isotopes in river suspended sediment depth-profiles: mixture of weathering** 336 **products and bedrock fragments**

337 The $\delta^7\text{Li}$ and Li/Al values of suspended sediments from river depth-profiles generally
338 plot below the negative correlation defined by RBS from the Amazon and Mackenzie
339 RBS (grey shaded region, Fig. 5a), and tend towards $\delta^7\text{Li}$ values lower than their

340 corresponding RBS (down to -3.5%). Each river profile defines specific Na/Al-Li/Al
341 and $\delta^7\text{Li}$ -Li/Al trends (represented by the arrows in Fig. 5a) with the lowest $\delta^7\text{Li}$ values
342 measured in surface sediments samples. As the dissolved lithium of the Amazon,
343 Mackenzie and Ganga-Brahmaputra rivers is enriched in ^7Li (Huh et al., 1998; Millot et
344 al., 2010), the present-day weathering processes are expected to produce a ^7Li -depleted
345 reservoir, complementary of the bedrock (and thus RBS) Li isotope composition. The low
346 Li isotope composition of large river suspended sediment suggests that SPM contains this
347 complementary reservoir as contemporary weathering products, likely mixed with
348 unweathered bedrock material. Weathering products are typically clays and Fe-Al oxides,
349 *i.e.* fine particles that we expect to be most enriched in the finest river SPM fraction,
350 sampled at the surface of the river. However, the finest river fraction is not necessarily
351 the pure weathering product, as it might also contain fine un-weathered bedrock
352 fragments. In a given river, the finest river sample does give the closest measured
353 constraint on the elemental and isotopic composition of the pure weathering product.
354 However, one can go further by assuming that Na, which is one of the most mobile
355 elements during chemical weathering (Gaillardet et al., 2003), is not incorporated into
356 secondary products. Therefore, in mixing diagrams Na/Al vs. Li/Al and $\delta^7\text{Li}$ vs. Na/Li,
357 trends formed by river depth-profiles can be extrapolated to Na=0 to infer the Li/Al and
358 $\delta^7\text{Li}$ values of a theoretical fully weathered component (Fig. 6).

359 For each river, the extrapolated chemical and isotopic composition of the weathering
360 product component should be compatible with what is known about the behavior of Li
361 and its isotopes during weathering. The Beni River, a tributary of the Madeira River (Fig.
362 1a), represents a simple study case as this river mostly drains sedimentary rocks. The

363 Beni SPM depict a pattern of ^7Li - and Li-depletion in the SPM with decreasing sampling
364 depth (Fig. 5b), illustrating a mixture between coarse materials with a composition close
365 to a shale-type bedrock, and a ^6Li -enriched fine component corresponding to the present-
366 day shale weathering product. For this case, we can independently predict the evolution
367 of $\delta^7\text{Li}$ values of the solid phase during weathering expected from the transformation of
368 igneous and sedimentary rocks into secondary minerals, using a two-step weathering
369 model taken from Vigier et al. (2009). The first step corresponds to bedrock dissolution
370 with no Li isotope fractionation, and the second to formation of solid weathering products
371 with an apparent fractionation factor [$\alpha_{\text{product-dissolved}} = (^7\text{Li}/^6\text{Li})_{\text{product}} / (^7\text{Li}/^6\text{Li})_{\text{dissolved}}$]. The
372 $\alpha_{\text{product-dissolved}}$ values available in the literature span a range from 0.972 to 1.000 (see
373 Burton and Vigier 2011 for a review). These fractionation factors are either determined
374 experimentally or derived from field studies and reflect both adsorption or precipitation
375 processes. Only two experimental studies have been conducted at various temperatures
376 (Millot et al., 2010; Vigier et al., 2008) and fractionation factors for the temperature
377 between 0 and 30°C range between 0.979 and 0.984. In addition, fractionation factors
378 determined by the study of the dissolved load of the Mackenzie River ranges from 0.985
379 to 0.987 (Millot et al., 2010; Tipper et al., 2012) and for the Amazon River from 0.982 to
380 0.989 (Dellinger et al., 2013). Therefore, we use in the following a fractionation factor of
381 0.985 ± 0.006 . The uncertainty allows us to account for a range of likely fractionation
382 factors values, which may be refined by future work.

383

384 Classically, in an open system, two extreme fractionation scenarios can be proposed to
385 model isotope fractionation in the weathering zone (Bouchez et al., 2013; Georg et al.,

386 2007), a "batch" model (in which solid secondary products and the liquid phase remain in
 387 contact) and a "Rayleigh distillation" model (where the liquid phase is continuously
 388 removed from the system and hence cannot interact with the solid once formed). The
 389 "batch" and "Rayleigh distillation" weathering scenarios correspond respectively to
 390 equations 1 and 2:

$$391 \quad \delta^7 Li_{product} = \delta^7 Li_{rock} + 1000 \times (1 - F_{Li}) \times \ln(\alpha_{product-dissolved}) \quad (1)$$

$$392 \quad \delta^7 Li_{product} = \left(\left(\frac{\delta^7 Li_{rock}}{1000} + 1 \right) \times \left(\frac{(1 - F_{Li})^{\alpha_{product-dissolved}} - 1}{-F_{Li}} \right) - 1 \right) \times 1000 \quad (2)$$

393 where $\delta^7 Li_{dissolved}$, $\delta^7 Li_{product}$, $\delta^7 Li_{rock}$ are the Li isotope compositions of the solution, of
 394 secondary weathering products and of the initial rock respectively and F_{Li} is the fraction
 395 of Li removed from solution (i.e. incorporated into weathering products during their
 396 precipitation). Assuming that dissolved Al concentration is negligible which is the case in
 397 the majority of the Earth's rivers (Gaillardet et al., 2003), F_{Li} can be expressed as
 398 $(Li/Al)_{product} / (Li/Al)_{rock}$ and then the trends predicted by equations (1) and (2) can be
 399 represented in $\delta^7 Li$ vs. Li/Al diagrams. Sensitivity tests show that within the range of F_{Li}
 400 and $\alpha_{product-dissolved}$ considered here, the difference between the two types of fractionation
 401 models does not lead to isotopic differences larger than 4%. We find that the weathering
 402 models can reproduce the composition of the Beni River fine component (determined
 403 using the method of extrapolation to Na concentration = 0) provided that $70 \pm 15\%$ of
 404 solubilized Li is incorporated into solid secondary products (Fig. 6).

405 In the Mackenzie watershed, SPM samples generally plot on or close to the RBS
 406 correlation between igneous rocks and shales. It appears that bedrock heterogeneity rather
 407 than modern weathering processes mostly control their chemical and isotopic variability.

408 This is entirely consistent with the very low degree of silicate weathering and low-
409 temperature conditions in the Mackenzie watershed (Millot et al., 2010), but precludes
410 the use of the weathering model developed here.

411 Interpretation of depth-profiles data for the other rivers (*e.g.* Solimões, Liard or Ganga) is
412 less straightforward. Most of them show a decrease of $\delta^7\text{Li}$ values in SPM towards the
413 surface of the depth-profiles, associated with an increase of the Li/Al ratio, thus a Li-
414 enrichment (Fig. 5a). This feature appears as a conundrum, given the soluble nature of Li.
415 We would indeed have expected that chemical weathering would deplete the fine
416 suspended sediments in both Li and ^7Li . However, in a similar manner to the more simple
417 case of the Beni River, SPM sampled along depth-profiles of these large rivers can be
418 interpreted as a mixture between a coarse, bedrock-like component and a fine component
419 which itself is a mixture of (a) present-day weathering products of both shale and igneous
420 or high-grade metamorphic rocks (for the G-B rivers) and (b) unweathered, mechanically
421 eroded, sedimentary rock particles. In other words, the fine suspended sediments of the
422 Solimões are enriched in Li compared to RBS because they contain a higher proportion
423 of Li-rich shale-derived particles (even if some Li has been solubilized by modern
424 weathering processes) than coarse sediments. The geological context supports this
425 interpretation, as these drainage areas are composed of mixed igneous and sedimentary
426 lithologies.

427 Therefore, Li isotopes in large river sediment reflect several processes:

- 428 (a) Modern weathering processes, as the fine fraction of river sediments is depleted in ^7Li
429 and contains the complementary reservoir of the dissolved lithium.
- 430 (b) Contribution of the different rock sources, especially in coarse sediments rich in rock

431 fragments.

432 (c) Impact of ancient weathering episodes as they record the contribution of recycled
433 sedimentary rocks.

434

435 In the following section, we quantify the relative contributions of these different
436 components (unweathered igneous, high-grade meta-sedimentary rocks, and sedimentary
437 rock fragments, and respective weathering products) to the solid material transported by
438 large rivers in order to discuss the relative importance of sedimentary recycling and
439 modern weathering processes.

440

441 **5.3 An inverse model to calculate the proportion of present-day versus inherited**
442 **weathering products in river sediments.**

443 The proportions of “new” (present-day weathering products) versus “old” (inherited
444 weathering products) material in river particulates can be determined based on a set of
445 mass budget equations using Na/Al, Li/Al ratios and $\delta^7\text{Li}$ values. The Li isotope
446 composition of river sediments reflects the contribution of six end-members: igneous
447 rocks, shales (low-grade meta-sedimentary rocks), high-grade meta-sedimentary rocks
448 and the three associated weathering products. In the Amazon and Mackenzie basins, the
449 contribution of the high-grade metamorphic end-member is negligible because i)
450 metamorphic rock outcrops are scarce in the sediment source area and ii) Mackenzie and
451 Amazon river sands define simple relationships in Na/Al-Li/Al and $\delta^7\text{Li}$ -Li/Al diagrams
452 (Fig. 4) that are compatible with a mixing between only two end-members (sedimentary
453 and igneous rocks). In the G-B river system, the dominant source of suspended sediment

454 is the HHC formation corresponding to high-grade meta-sedimentary rocks, with the
 455 remaining sediments deriving from low-grade sedimentary rocks with minor contribution
 456 from igneous rocks (such as leucogranites) (Galy and France-Lanord, 2001). As a result,
 457 for all the river systems studied here, each calculation is done with only four end-
 458 members.

459 Importantly, these end-members will be valid for any river sediment from a depth-profile,
 460 but also for the coarse and fine component of the depth-profile. Such mixtures can be
 461 expressed with a series of coupled mixing equations. For the river coarse component:

$$462 \quad \left(\frac{Li}{Al}\right)_{coarse} = \sum_i \left(\frac{Li}{Al}\right)_i \times \gamma_i(Al) \quad (3)$$

$$463 \quad \left(\frac{Na}{Al}\right)_{coarse} = \sum_i \left(\frac{Na}{Al}\right)_i \times \gamma_i(Al) \quad (4)$$

$$464 \quad \delta^7 Li_{coarse} = \sum_i \delta^7 Li_i \times \left(\frac{\left(\frac{Li}{Al}\right)_i}{\left(\frac{Li}{Al}\right)_{coarse}} \right) \times \gamma_i(Al) \quad (5)$$

465 with γ_i = the proportion of Al from each lithology in the coarse end-member, i = shale (S)
 466 and igneous (I) (or high-grade meta-sedimentary rocks (HG) for the G-B). The
 467 contribution of modern weathering products in the coarse component is most likely small
 468 for the reasons developed in section (5.1) and thus can be neglected here.

469 For the fine component:

$$470 \quad \left(\frac{Li}{Al}\right)_{fine} = \sum_j \left(\frac{Li}{Al}\right)_j \times \beta_j(Al) \quad (6)$$

471
$$\left(\frac{Na}{Al}\right)_{fine} = \sum_j \left(\frac{Na}{Al}\right)_j \times \beta_j(Al) \quad (7)$$

472
$$\delta^7 Li_{fine} = \sum_j \delta^7 Li_i \times \left(\frac{\left(\frac{Li}{Al}\right)_j}{\left(\frac{Li}{Al}\right)_{fine}}\right) \times \beta_j(Al) \quad (8)$$

473 With β_i = the proportion of Al from each end member, j = unweathered fine-grained
 474 shales (FGS) and shale weathering products (SWP), and igneous weathering products
 475 (IWP) (or high-grade metasedimentary rocks weathering products, HGWP) for the G-B.
 476 Mass balance calculation using the Na/Al ratio show that the contribution of the
 477 unweathered igneous and high-grade metasedimentary rocks to the fine component is low
 478 (7% maximum), and hence can be neglected. Mass conservation implies that:

479
$$\sum_i \gamma_i(Al) = 1 \quad (9)$$

480 and

481
$$\sum_j \beta_j(Al) = 1 \quad (10)$$

482 Any sample from a river SPM depth-profile can be described as a mixture between the
 483 coarse and the fine components, or equivalently as a mixture of the four end-members
 484 described above. To account for this, mixing equations can be written for SPM:

485

486
$$\left(\frac{Li}{Al}\right)_{SPM} = \left(\frac{Li}{Al}\right)_{Coarse} \times \mu_{coarse}(Al) + \left(\frac{Li}{Al}\right)_{fine} \times \mu_{fine}(Al) \quad (11)$$

487
$$\left(\frac{Na}{Al}\right)_{SPM} = \left(\frac{Na}{Al}\right)_{Coarse} \times \mu_{coarse}(Al) + \left(\frac{Na}{Al}\right)_{fine} \times \mu_{fine}(Al) \quad (12)$$

488
$$\delta^7 Li_{SPM} = \delta^7 Li_{coarse} \times \left(\frac{\left(\frac{Li}{Al}\right)_{coarse}}{\left(\frac{Li}{Al}\right)_{SPM}}\right) \times \mu_{coarse}(Al) + \delta^7 Li_{fine} \times \left(\frac{\left(\frac{Li}{Al}\right)_{fine}}{\left(\frac{Li}{Al}\right)_{SPM}}\right) \times \mu_{fine}(Al) \quad (13)$$

489 Where the subscripts “coarse” and “fine” denote the coarse and fine components
 490 respectively. μ_{coarse} and μ_{fine} are the proportion of Al in the coarse and fine components
 491 respectively. In the following, we use the depth-integrated composition for the Li/Al and
 492 Na/Al ratio and $\delta^7 Li$ of the representative sediment sample. Mass conservation implies
 493 that:

494
$$\mu_{coarse} + \mu_{fine} = 1 \quad (14)$$

495 It should be emphasized that the mixing proportions calculated by the model (γ_i , β_i ,
 496 μ_{coarse} , μ_{fine}) represent the contribution of the different end-members to the Al budget of
 497 river sediments, and not to the total river sediment mass. However, given that Al
 498 concentration is not very different between sediments and parent bedrocks, the mixing
 499 proportions can be considered, within error, as contributions of the different reservoirs to
 500 total sediment mass.

501 A fourth set of model equations corresponds to those of the fractionation model
 502 (equations 1 and 2). These equations constrain the Li isotopic composition of the
 503 weathering product end-members for each rock type, by using the Rayleigh and/or batch
 504 model and an isotope fractionation factor of 0.985 (± 0.006).

505 The full set of equations constitutes an overdetermined system. Some of the parameters
506 of the mixing model have a large uncertainty, while others are relatively well known (see
507 supplementary informations for details). The equations are solved by an inverse method
508 well suited for such a situation. The mathematical technique of data inversion was first
509 popularized in geochemistry for mantle studies (Allègre et al., 1983; Allègre and Lewin,
510 1989), and have been applied to interpret chemical weathering processes from the
511 dissolved and particulate loads of rivers (Gaillardet et al., 1995; Gaillardet et al., 1999a).
512 In a proper inversion procedure, all parameters (called the *a priori* parameters) are
513 attributed a mean value and an associated uncertainty that quantify our degree of
514 knowledge of the parameter Here, the least-known parameters are the mixing proportions
515 and the composition of the weathering product end-members. The best-known parameters
516 are the chemical and isotopic ratios measured along the river depth-profiles. The
517 inversion algorithm iteratively modifies the parameter values and errors as it tries to find
518 a unique solution so that all the parameters values fit (in the sense of least squares) the
519 imposed model equations. The inversion is successful (converges) when the algorithm
520 finds a unique set of *a posteriori* parameters satisfying all model equations and improves
521 the uncertainty on the least-constrained parameters (Gaillardet et al., 1995).

522 The inversion was run on the river samples where the depth-profiles were available
523 (for the Slave and Pastaza-Napo rivers, only surface SPM were sampled). In all cases, the
524 inversion procedure converged on a solution, *i.e.* a set of *a posteriori* parameters
525 fulfilling all the model equations. The gain of information (calculated by comparing *a*
526 *posteriori* uncertainties with *a priori* uncertainties) was the most important on the mixing
527 proportions. *A priori* and *a posteriori* parameters are given in Table (S1). The inversion

528 was run using the two extreme scenarios (batch and Rayleigh fractionation model) and
529 gave relatively similar mixing proportion regarding the different models. Results are
530 summarized in Table (S1) and Fig. (7). The model sensitivity to the *a priori* values of the
531 parameters was tested by testing the “elasticity of the parameters” as defined by Allègre
532 and Lewin (1989). The *a priori* value of each parameter was changed (by half the *a priori*
533 associated uncertainty) one after the other. For each modified *a priori* parameter the
534 inversion model was run again to calculate a new set of *a posteriori* values. For example,
535 for the Solimões River, the $\delta^7\text{Li}_{\text{fine}} = -3.8 \pm 0.8\text{‰}$ was changed to $-3.4 \pm 0.8\text{‰}$ and -
536 $4.20 \pm 0.8\text{‰}$, or the $\delta^7\text{Li}_{\text{SWP}} = -7 \pm 4\text{‰}$ was changed to $-9 \pm 4\text{‰}$ and $-5 \pm 4\text{‰}$. The new *a*
537 *posteriori* parameters were compared to the result of the “reference inversion” (parameter
538 values of Table S1). As a result, the mixing proportions were changed by less than 0.05.
539 This sensitivity analysis shows that our findings do not depend strongly on the chosen
540 values of the parameters and that the inversion procedure is robust.

541

542 **5.4 Results of the inverse model and potential implications.**

543 The inverse model presented above sheds new light over weathering processes and
544 erosion as inferred from large river systems.

545 (1) The first important overall result is that river particulates, at least in the Amazon,
546 Mackenzie and Ganga-Brahmaputra river systems, are preferentially derived (more than
547 60% for most rivers) from the erosion and weathering of sedimentary rocks. This source
548 information is consistent with the geochemical mass budget of major and trace elements
549 (Gaillardet et al., 1999b). Li isotopes therefore confirm the cannibalistic nature (Veizer
550 and Jensen, 1985) of continental erosion as the majority of river particulates that will

551 further accumulate in the ocean are derived from a reservoir formed by ancient weathered
552 material. In turn, Li isotopes indicate that 40% of the river particulates are sourced from
553 igneous rocks. Within the Amazon watershed the different proportions calculated by the
554 inversion procedure for the Solimoes (38 % of sedimentary-derived material) and
555 Madeira rivers (91 %) are in good agreement with geological evidence, as more igneous
556 rocks are present in the Solimoes watershed. The preferential transport of old sedimentary
557 sourced material in the suspended load of large rivers reflects the abundance of
558 sedimentary rocks at the Earth surface, especially in active mountain belts, where these
559 rocks have been uplifted and where their preferential erosion is facilitated by their high
560 erodibility.

561 (2) The second relevant information deduced from the inversion of Li isotopic data is that
562 present-day chemical weathering products account for less than 35% of the SPM
563 transported by the Mackenzie, G-B and Amazon rivers (relative uncertainty of $\pm 15\%$).
564 This means that most of the river particulates ($> 65\%$ of total SPM) have been mobilized
565 by physical erosion processes without undergoing any significant present-day chemical
566 weathering. Out of these present-day weathering products, those sourced from old
567 sedimentary rocks are more important than secondary minerals produced by weathering
568 of igneous rocks. As shown in the Fig. (7), within errors, the proportions of « new »
569 weathered material is fairly uniform across the different rivers investigated here. The
570 relatively modest fingerprint of present-day chemical weathering reactions in large river
571 suspended sediments is probably due to the poor chemical reactivity of sedimentary rocks
572 in contact with water. Sedimentary rocks have already been exposed to surface processes
573 during ancient weathering episodes and the new phases formed at that time are relatively

574 stable under the conditions of the Earth surface (Condie, 1993; Holland, 1984). In
575 addition, large outcrops of sedimentary rocks have been uplifted in high-elevation
576 mountain ranges where rapid erosion and therefore short residence time in the weathering
577 zone preclude high chemical weathering intensity (“weathering-limited” regimes). One
578 implication of this result is that, in order to use large river SPM to understand present-day
579 weathering processes, the recycling of old weathered material must be taken into account.
580 In particular, it is not possible to determine isotopic fractionation factors during chemical
581 weathering by comparing river dissolved and bulk suspended loads without separating the
582 “old” from the “new” weathered component in suspended material (in addition to
583 separating the primary from the secondary component).

584 Our results also show that the finest river sediments, found at the top of the depth profiles
585 are more influenced by present-day weathering processes with regards to Li isotopes than
586 sediments found at greater depths. An important consequence of the inversion of Li
587 isotopic data in river sediments is that the sampling of suspended sediments just below
588 the surface of large rivers (as done in most studies) therefore introduces an important bias
589 toward the weathered component of suspended material.

590 Finally, our quantification of the source of present-day weathering products using Li
591 isotopes may have important implications for the geological carbon cycle. While the
592 consumption of atmospheric CO₂ has not been quantified here, silicate minerals in meta-
593 sedimentary rocks are generally depleted in base cations such as Ca and Mg (Condie,
594 1993), which means that their weathering might not result in an efficient sink of
595 atmospheric CO₂ when compared to the weathering of igneous rocks. This implies that
596 recycling during continental erosion and weathering may limit the capacity of

597 sedimentary-rock dominated orogens for atmospheric CO₂ consumption. Indeed,
598 although increased silicate weathering rates are expected during mountain building in
599 regions where temperature is warm enough and water supply high enough to fuel
600 chemical weathering (West et al., 2005; West 2012), the strength of this process may be
601 reduced if most of the exhumed rocks are base cation-depleted. In that case, cation-rich
602 volcanic islands and basaltic provinces would likely represent the most efficient
603 geodynamic settings to regulate climate through chemical weathering (Dupré et al.,
604 2003).

605

606 **6. Conclusions**

607 Based on the correlation between sediment grain size, Li content and Li isotope
608 composition in the sediments carried by the Amazon, Mackenzie and Ganga-
609 Brahmaputra rivers, we show that these large rivers mostly recycle sedimentary material.
610 This confirms the hypothesis that the present-day erosion cycle is dominantly
611 cannibalistic in nature (Veizer and Jansen, 1979, 1985). Using a mass budget approach on
612 the river sediments with the Li, Na content and Li isotope composition, an inverse
613 method quantifies the degree of cannibalism (for the Amazon, Mackenzie and G-B rivers)
614 to be between 60% to 85%, in reasonable agreement with the estimate (90 %) based on
615 the study of Nd isotope in shales (Veizer and Jansen, 1985).

616 The variation of Li isotope composition in river sediment depth-profiles of large rivers
617 therefore integrates the weathering history of the continental crust over long periods of
618 time. Modern weathering products are mixed with those inherited from ancient
619 weathering episodes. The time-integrated view offered by river depth-profiles (similarly

620 to that offered by soil profiles, but over much longer timescales) is in contrast to the
621 “snapshot” insight provided by river dissolved load on present-day weathering processes.

622

623

624 **Acknowledgments.** This paper gained from constructive comments on the original
625 manuscript by Claude Hillaire-Marcel and Pierre Cartigny. Jean Louis Birck, Edward
626 Tipper, Alkis Gourgiotis, Julien Moureau, Romain Millot, Bassam Ghaleb and Nathalie
627 Vigier are thanked for discussions and analytical assistance. We also thank Philip Pogge
628 von Strandmann, an anonymous reviewer and editor Tim Elliott for comments that
629 greatly improved this manuscript. MD benefited from a Canadian-French joint PhD grant.

630 This study was funded by the CNRS-INSU program Syster. This is IPGP contribution
631 XXX.

632

633 **References:**

634

635 Allègre, C.J., Hart, S., Minster, J.-F., 1983. Chemical structure and evolution of the
636 mantle and continents determined by inversion of Nd and Sr isotopic data, II.
637 Numerical experiments and discussion. *Earth Planet. Sci. Let.* 66, 191-213.

638

639 Allègre, C.J., Lewin, E., 1989. Chemical structure and history of the Earth: evidence
640 from global non-linear inversion of isotopic data in a three-box model. *Earth Planet.*
641 *Sci. Let.* 96, 61-88.

642

643 Berner, R.A., Lasaga, A.C., Garrels, R.M., 1983. The carbonate-silicate geochemical
644 cycle and its effect on atmospheric carbon dioxide over the past 100 million years.
645 *Am. J. Sci.* 283, 641-683.

646

647 Bouchez, J., Gaillardet, J., France-Lanord, C., Maurice, L., Dutra-Maia, P., 2011a. Grain
648 size control of river suspended sediment geochemistry: Clues from Amazon River
649 depth profiles. *Geochem. Geophys. Geosyst.* 12, Q03008.

650

651 Bouchez, J., Gaillardet, J., Lupker, M., Louvat, P., France-Lanord, C., Maurice, L.,
652 Armijos, E., Moquet, J.-S., 2012. Floodplains of large rivers: Weathering reactors or
653 simple silos? *Chem. Geol.* 332–333, 166-184.

654
655 Bouchez, J., Lupker, M., Gaillardet, J., France-Lanord, C., Maurice, L., 2011b. How
656 important is it to integrate riverine suspended sediment chemical composition with
657 depth? Clues from Amazon River depth-profiles. *Geochim. et Cosmochim. Act.* 75,
658 6955-6970.
659
660 Bouchez, J., von Blanckenburg, F., Schuessler, J.A., 2013. Modeling novel stable
661 isotope ratios in the weathering zone. *Am. J. Sci.* 313, 267-308.
662
663 Burton, K.W., Vigier, N. 2012. Lithium Isotopes as tracers in Marine and terrestrial
664 environments. In *Handbook of Environmental Isotope Geochemistry* (pp. 41-59).
665 Springer Berlin Heidelberg.
666
667 Carson, M.A., Jasper, J.N., Conly, F.M., 1998. Magnitude and Sources of Sediment
668 Input to the Mackenzie Delta, Northwest Territories, 1974-94.
669
670 Condie, K.C., 1993. Chemical composition and evolution of the upper continental
671 crust: Contrasting results from surface samples and shales. *Chem. Geol.* 104, 1-37.
672
673 Dosseto, A., Bourdon, B., Gaillardet, J., Allègre, C.J., Filizola, N., 2006. Time scale and
674 conditions of weathering under tropical climate: Study of the Amazon basin with U-
675 series. *Geochim. et Cosmochim. Act.* 70, 71-89.
676
677 Dellinger, M., Gaillardet, J., Bouchez, J., Calmels D., Louvat, P., Gorge, C., Maurice, L.,
678 *Mineralogical Magazine*, 77(5) 967.
679
680 Dupré, B., Dessert, C., Oliva, P., Goddérès, Y., Viers, J., François, L., Millot, R., Gaillardet,
681 J., 2003. Rivers, chemical weathering and Earth's climate. *C.R. Geosci.* 335, 1141-
682 1160.
683
684 Franzinelli, E., Potter, P.E., 1983. Petrology, Chemistry, and Texture of Modern River
685 Sands, Amazon River System. *J. Geol.* 91, 23-39.
686
687 Gaillardet, J., Dupré, B., Allègre, C.J., 1995. A global geochemical mass budget applied
688 to the Congo Basin rivers: Erosion rates and continental crust composition.
689 *Geochim. et Cosmochim. Act.* 59, 3469-3485.
690
691 Gaillardet, J., Dupré, B., Allègre, C.J., 1999a. Geochemistry of large river suspended
692 sediments: silicate weathering or recycling tracer? *Geochim. et Cosmochim. Act.* 63,
693 4037-4051.
694
695 Gaillardet, J., Dupré, B., Louvat, P., Allègre, C.J., 1999b. Global silicate weathering and
696 CO₂ consumption rates deduced from the chemistry of large rivers. *Chem. Geol.* 159,
697 3-30.
698

699 Gaillardet, J., Viers, J., Dupré, B., 2003. Trace elements in river waters. *Treatise on*
700 *geochemistry*, 5, 225-272.
701
702 Galy, A., France-Lanord, C., 1999. Weathering processes in the Ganges–Brahmaputra
703 basin and the riverine alkalinity budget. *Chem. Geol.* 159, 31-60.
704
705 Galy, A., France-Lanord, C., 2001. Higher erosion rates in the Himalaya: Geochemical
706 constraints on riverine fluxes. *Geology* 29, 23-26.
707
708 Galy, V., France-Lanord, C., Beyssac, O., Faure, P., Kudrass, H., Palhol, F., 2007.
709 Efficient organic carbon burial in the Bengal fan sustained by the Himalayan
710 erosional system. *Nature* 450, 407-410.
711
712 Gardner, R., Walsh, N., 1996. Chemical weathering of metamorphic rocks from low
713 elevations in the southern Himalaya. *Chem. Geol.* 127, 161-176.
714
715 Georg, R.B., Reynolds, B.C., West, A.J., Burton, K.W., Halliday, A.N., 2007. Silicon
716 isotope variations accompanying basalt weathering in Iceland. *Earth Planet. Sci. Let.*
717 261, 476-490.
718
719 Gibbs, R. J., 1967. The geochemistry of the Amazon River system: Part I. The factors
720 that control the salinity and the composition and concentration of the suspended
721 solids. *GSA Bulletin.* 78, 1203-1232.
722
723 Heimsath, A.M., Dietrich, W.E., Nishiizumi, K., Finkel, R.C., 1997. The soil production
724 function and landscape equilibrium. *Nature.* 388, 358-361.
725
726 Hilton, R.G., Galy, A., Hovius, N., Horng, M.J., Chen, H., 2010. The isotopic composition
727 of particulate organic carbon in mountain rivers of Taiwan. *Geochim. et Cosmochim.*
728 *Act.* 74, 3164-3181.
729
730 Holland, H.D., 1984. *The Chemical Evolution of the Atmosphere and Oceans.*
731 Princeton University Press, Princeton, NJ.
732
733 Huh, Y., Chan, L.H., Edmond, J.M., 2001. Lithium isotopes as a probe of weathering
734 processes: Orinoco River. *Earth Planet. Sci. Let.* 194, 189-199.
735
736 Huh, Y., Chan, L.-H., Zhang, L., Edmond, J.M., 1998. Lithium and its isotopes in major
737 world rivers: implications for weathering and the oceanic budget. *Geochim. et*
738 *Cosmochim. Acta.* 62, 2039-2051.
739
740 James, R.H., Palmer, M. R. (2000). The lithium isotope composition of international
741 rock standards. *Chem. Geol.* 166(3), 319-326.
742
743 Kisakurek, B., James, R.H., Harris, N.B.W., 2005. Li and $\delta^7\text{Li}$ in Himalayan rivers:
744 Proxies for silicate weathering? *Earth Planet. Sci. Let.* 237, 387-401.

745
746 Kisakürek, B., Widdowson, M., James, R.H., 2004. Behaviour of Li isotopes during
747 continental weathering: the Bidar laterite profile, India. *Chem. Geol.* 212, 27-44.
748
749 Lee, C.-T.A., Morton, D.M., Little, M.G., Kistler, R., Horodyskyj, U.N., Leeman, W.P.,
750 Agranier, A., 2008. Regulating continent growth and composition by chemical
751 weathering. *Proc. Nati. Acad. Sci.* 105, 4981-4986.
752
753 Lemarchand, E., Chabaux, F., Vigier, N., Millot, R., Pierret, M.-C., 2010. Lithium
754 isotope systematics in a forested granitic catchment (Strengbach, Vosges Mountains,
755 France). *Geochim. et Cosmochim. Acta.* 74, 4612-4628.
756
757 Liu, X.-M., Rudnick, R.L., 2011. Constraints on continental crustal mass loss via
758 chemical weathering using lithium and its isotopes. *Proc. Nati. Acad. Sci.*, 3062.
759
760 Lupker, M., France-Lanord, C., Galy, V., Lavé, J., Gaillardet, J., Gajurel, A.P., Guilmette,
761 C., Rahman, M., Singh, S.K., Sinha, R., 2012. Predominant floodplain over mountain
762 weathering of Himalayan sediments (Ganga basin). *Geochim. et Cosmochim. Acta.* 84,
763 410-432.
764
765 Lupker, M., France-Lanord, C., Lavé, J., Bouchez, J., Galy, V., Mètivier, F., Gaillardet, J.,
766 Lartiges, B., Mugnier, J.-L., 2011. A Rouse-based method to integrate the chemical
767 composition of river sediments: Application to the Ganga basin. *J. Geophys. Res.* 116,
768 F04012.
769
770 Magna, T., Wiechert, U., Grove, T.L., Halliday, A.N., 2006. Lithium isotope
771 fractionation in the southern Cascadia subduction zone. *Earth Planet. Sci. Lett.* 250,
772 428-443.
773
774 Milliman, J.D., Farnsworth, K.L., 2011. *River Discharge to the Coastal Ocean.*
775 Cambridge University Press.
776
777 Millot, R., Gaillardet, J., Dupré, B., Allègre, C.J., 2003. Northern latitude chemical
778 weathering rates: clues from the Mackenzie River Basin, Canada. *Geochim. et*
779 *Cosmochim. Acta.* 67, 1305-1329.
780
781 Millot, R., Vigier, N., Gaillardet, J., 2010. Behaviour of lithium and its isotopes during
782 weathering in the Mackenzie Basin, Canada. *Geochim. et Cosmochim. Acta.* 74, 3897-
783 3912.
784
785 Millot, R., Scaillet, B., & Sanjuan, B. 2010. Lithium isotopes in island arc geothermal
786 systems: Guadeloupe, Martinique (French West Indies) and experimental approach.
787 *Geochim. et Cosmochim. Acta.* 74, 1852-1871.
788
789 Penniston-Dorland, S.C., Bebout, G.E., Pogge von Strandmann, P.A.E., Elliott, T.,
790 Sorensen, S.S., 2012. Lithium and its isotopes as tracers of subduction zone fluids

791 and metasomatic processes: Evidence from the Catalina Schist, California, USA.
792 *Geochim. et Cosmochim. Acta.* 77, 530-545.
793
794 Pistiner, J.S., Henderson, G.M., 2003. Lithium-isotope fractionation during
795 continental weathering processes. *Earth Planet. Sci. Lett.* 214, 327-339.
796
797 Pogge von Strandmann, P.A.E., Opfergelt, S., Lai, Y.-J., Sigfússon, B., Gislason, S.R.,
798 Burton, K.W., 2012. Lithium, magnesium and silicon isotope behaviour
799 accompanying weathering in a basaltic soil and pore water profile in Iceland. *Earth*
800 *Planet. Sci. Lett.* 339, 11-23.
801
802 Pogge von Strandmann, P.A.E., Burton, K.W., James, R.H., van Calsteren, P., Gislason,
803 S.R., 2010. Assessing the role of climate on uranium and lithium isotope behaviour
804 in rivers draining a basaltic terrain. *Chem. Geol.* 270, 227-239.
805
806 Potter, P.E., 1978. Petrology and Chemistry of Modern Big River Sands. *The Journal*
807 *of Geology* 86, 423-449.
808
809 Qiu, L., Rudnick, R.L., Ague, J.J., McDonough, W.F., 2011a. A lithium isotopic study of
810 sub-greenschist to greenschist facies metamorphism in an accretionary prism, New
811 Zealand. *Earth Planet. Sci. Lett.* 301, 213-221.
812
813 Qiu, L., Rudnick, R.L., McDonough, W.F., Bea, F., 2011b. The behavior of lithium in
814 amphibolite- to granulite-facies rocks of the Ivrea-Verbano Zone, NW Italy. *Chem.*
815 *Geol.* 289, 76-85.
816
817 Qiu, L., Rudnick, R.L., McDonough, W.F., Merriman, R.J., 2009. Li and $\delta^7\text{Li}$ in
818 mudrocks from the British Caledonides: Metamorphism and source influences.
819 *Geochim. et Cosmochim. Acta.* 73, 7325-7340.
820
821 Raymo, M.E., Ruddiman, W.F., Froelich, P.N., 1988. Influence of late Cenozoic
822 mountain building on ocean geochemical cycles. *Geology* 16, 649-653.
823
824 Rudnick, R.L., 1995. Making continental crust. *Nature* 378, 571-578.
825
826 Rudnick, R.L., Tomascak, P.B., Njo, H.B., Gardner, L.R., 2004. Extreme lithium isotopic
827 fractionation during continental weathering revealed in saprolites from South
828 Carolina. *Chem. Geol.* 212, 45-57.
829
830 Schuessler, J.A., Schoenberg, R., Sigmarsson, O., 2009. Iron and lithium isotope
831 systematics of the Hekla volcano, Iceland — Evidence for Fe isotope fractionation
832 during magma differentiation. *Chem. Geol.* 258, 78-91.
833
834 Teng, F.Z., McDonough, W.F., Rudnick, R.L., Dalpé, C., Tomascak, P.B., Chappell, B.W.,
835 Gao, S., 2004. Lithium isotopic composition and concentration of the upper
836 continental crust. *Geochim. et Cosmochim. Acta.* 68, 4167-4178.

837
838 Teng, F.Z., Rudnick, R.L., McDonough, W.F., Wu, F.-Y., 2009. Lithium isotopic
839 systematics of A-type granites and their mafic enclaves: Further constraints on the
840 Li isotopic composition of the continental crust. *Chem. Geol.* 262, 370-379.
841
842 Tipper, E.T., Calmels, D., Gaillardet, J., Louvat, P., Capmas, F., Dubacq, B., 2012.
843 Positive correlation between Li and Mg isotope ratios in the river waters of the
844 Mackenzie Basin challenges the interpretation of apparent isotopic fractionation
845 during weathering. *Earth Planet. Sci. Let.* 333–334, 35-45.
846
847 Tomascak, P.B., Langmuir, C.H., le Roux, P.J., Shirey, S.B., 2008. Lithium isotopes in
848 global mid-ocean ridge basalts. *Geochim. et Cosmochim. Acta.* 72, 1626-1637.
849
850 Veizer, J., Jansen, S.L., 1979. Basement and Sedimentary Recycling and Continental
851 Evolution. *J. Geol.* 87, 341-370.
852
853 Veizer, J., Jansen, S.L., 1985. Basement and Sedimentary Recycling-2: Time
854 Dimension to Global Tectonics. *J. Geol.* 93, 625-643.
855
856 Vigier, N., Decarreau, A., Millot, R., Carignan, J., Petit, S., France-Lanord, C., 2008.
857 Quantifying Li isotope fractionation during smectite formation and implications for
858 the Li cycle. *Geochim. et Cosmochim. Acta.*, 72, 780-792.
859
860 Vigier, N., Gislason, S.R., Burton, K.W., Millot, R., Mokadem, F., 2009. The relationship
861 between riverine lithium isotope composition and silicate weathering rates in
862 Iceland. *Earth Planet. Sci. Let.* 287, 434-441.
863
864 Vital, H., Stattegger, K., 2000. Major and trace elements of stream sediments from
865 the lowermost Amazon River. *Chem. Geol.* 168, 151-168.
866
867 Wang, Q., Liu, C., Zhao, Z., Chetelat, B., and Ding, H., 2008. Lithium isotopic
868 composition of the dissolved and suspended loads of the Yangtze River, China. *Adv.*
869 *Earth Sci.* 23, 952–958
870
871 Walker, J.C.G., Hays, P.B., Kasting, J.F., 1981. A negative feedback mechanism for the
872 long-term stabilization of earth's surface temperature. *J. Geophys. Res.* 86, 9776-
873 9782.
874
875 West, A.J., Galy, A., Bickle, M., 2005. Tectonic and climatic controls on silicate
876 weathering. *Earth Planet. Sci. Let.* 235, 211-228.
877
878 West, A.J., 2012. Thickness of the chemical weathering zone and implications for
879 erosional and climatic drivers of weathering and for carbon-cycle feedbacks.
880 *Geology*, 40, 811-814.
881

882 Wimpenny, J., James, R.H., Burton, K.W., Gannoun, A., Mokadem, F., Gíslason, S.R.,
883 2010. Glacial effects on weathering processes: New insights from the elemental and
884 lithium isotopic composition of West Greenland rivers. *Earth Planet. Sci. Let.* 290,
885 427-437.

886
887 Wittmann, H., von Blanckenburg, F., Guyot, J.L., Laraque, A., Bernal, C., Kubik, P.W.,
888 2011a. Sediment production and transport from in situ-produced cosmogenic ^{10}Be
889 and river loads in the Napo River basin, an upper Amazon tributary of Ecuador and
890 Peru. *J. South Am. Earth Sci.* 31, 45-53.

891
892 Wittmann, H., von Blanckenburg, F., Maurice, L., Guyot, J.-L., Filizola, N., Kubik, P.W.,
893 2011b. Sediment production and delivery in the Amazon River basin quantified by
894 in situ-produced cosmogenic nuclides and recent river loads. *GSA Bulletin.* 123,
895 934-950.

896
897
898

899 **Figure captions**

900

901 **Fig. 1:** Map showing the location of the river basins and the samples.

902

903 **Fig. 2:** Example of typical river-profiles of (A) Li isotope composition versus d/H (the
904 sample position in the river depth-profile with d : sampling depth and H : channel depth)
905 for the Solimões, Madeira, Liard, Peel and Ganga rivers and (B) Li concentrations versus
906 d/H .

907

908 **Fig. 3.** Li isotope composition of river sediments as a function of Al/Si ratio, used here as
909 a proxy for grain size. Samples with low Al/Si (< 0.15) are river bed sands (squares)
910 while high- Al/Si samples are suspended sediments (circles). Data for each river depth-
911 profile align along a mixing hyperbola. The green and orange dotted curves correspond to
912 examples of calculated mixing hyperbola between coarse and fine sediments for the
913 Solimões and Madeira rivers, respectively.

914

915 **Fig. 4.** (A) Na/Al and (B) $\delta^7\text{Li}$ vs. Li/Al ratio for the Amazon and Mackenzie tributaries
916 and Ganga-Brahmaputra bed sediment samples (RBS). The Mackenzie and Amazon RBS
917 data can be fitted by a least-square mixing hyperbola (solid line, with grey error envelope
918 at 95% confidence) corresponding to the binary mixture between igneous and
919 sedimentary rocks having similar ranges of Li/Al and Na/Al as those defined in the
920 studies of Condie (1993) and Holland (1984). End-members are, for the igneous rock
921 component, $\text{Li/Al} \approx 0.30 \times 10^{-3}$, $\text{Na/Al} \approx 0.32$ and $\delta^7\text{Li} \approx +4.5\%$, and for the shale
922 component $\text{Li/Al} \approx 0.95 \times 10^{-3}$, $\text{Na/Al} \approx 0.08$ and $\delta^7\text{Li} \approx -0.5\%$. The high-grade meta-
923 sedimentary rock end-member is defined by the trend and values from the literature (Galy
924 and France-Lanord, 2001; Gardner and Walsh, 1996; Penniston-Dorland et al., 2012).

925

926 **Fig. 5.** (A) $\delta^7\text{Li}$ vs. Li/Al ratio for the Amazon and Mackenzie tributaries and Ganga-
927 Brahmaputra SPM and RBS samples. The arrows represent the sediment depth-profile
928 trends (from the bottom to the surface of the water column) of the main river samples. (B)
929 Close-up on the sedimentary rocks-dominated river basins where the enrichment of ^6Li of
930 particles is associated to a loss of Li. (C) Conceptual model proposed to explain the $\delta^7\text{Li}$
931 of river sediments applied to the Beni and Solimões river depth profiles (yellow and
932 green curves). In this diagram, mixtures between end-members are represented by
933 hyperbolae. The bold grey dotted curves represent theoretical calculated Li isotopic
934 composition of weathering products (batch and Rayleigh distillation models) with an
935 average isotope fractionation factor $\alpha_{\text{product-dissolved}} = 0.985$. The hexagons correspond to
936 the finest end-member estimated for the river depth profiles. Each sample can be

937 described as a mixture between the four end-members.

938

939 **Fig. 6:** (A) Li/Al vs Na/Al ratio and (B) $\delta^7\text{Li}$ vs. Na/Li for the Beni and Solimões rivers
940 depth-profile. These diagrams are used to estimate the composition of the fine component
941 between the surface SPM composition and a purely weathered component assumed to
942 contain no Na.

943

944 **Fig. 7.** Results of the mass-balance mixing model giving the proportions of unweathered
945 rock end-member (shales, igneous and high-grade meta-sedimentary rocks) and those of
946 modern weathering product end-members calculated by the inversion method for each
947 river system. The red line delineates the proportions of unweathered material from those
948 of contemporaneous products of weathering.

949

950

951

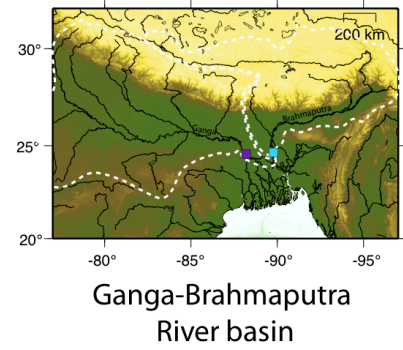
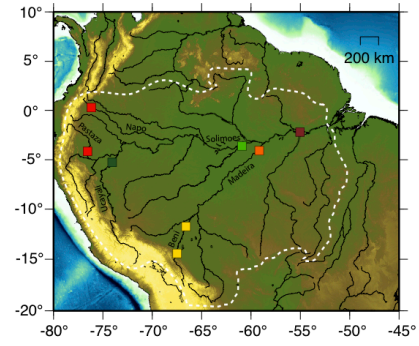
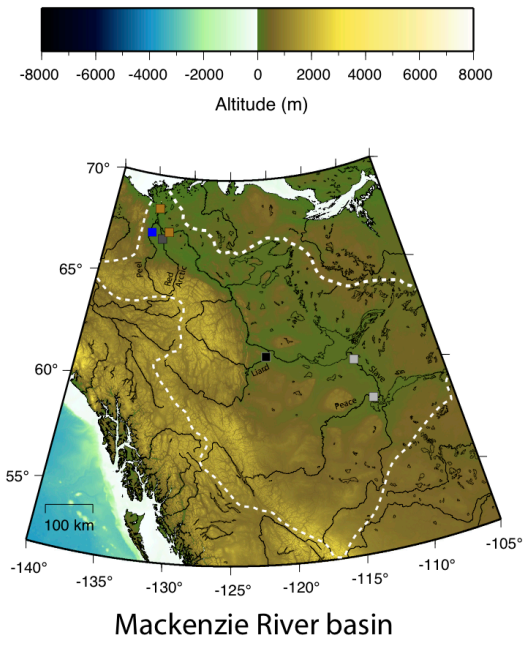


Figure 1

- 952
- 953
- 954
- 955
- 956
- 957
- 958
- 959
- 960
- 961
- 962
- 963
- 964

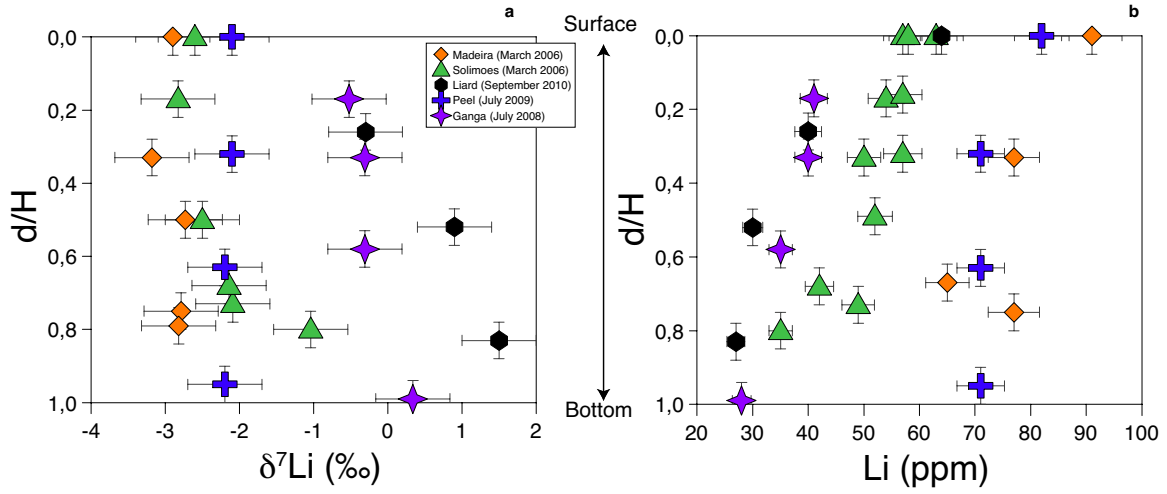


Figure 2

965

966

967

968

969

970

971

972

973

974

975

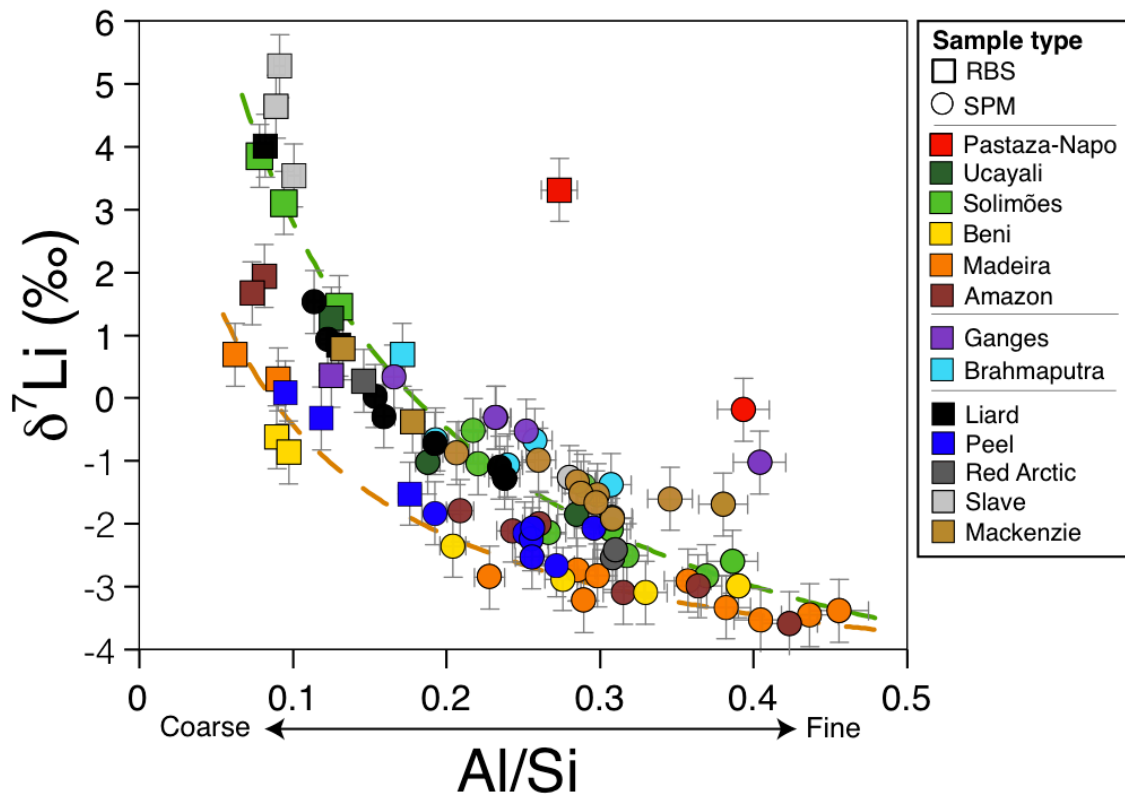
976

977

978

979

980



981

982

983

984

Figure 3

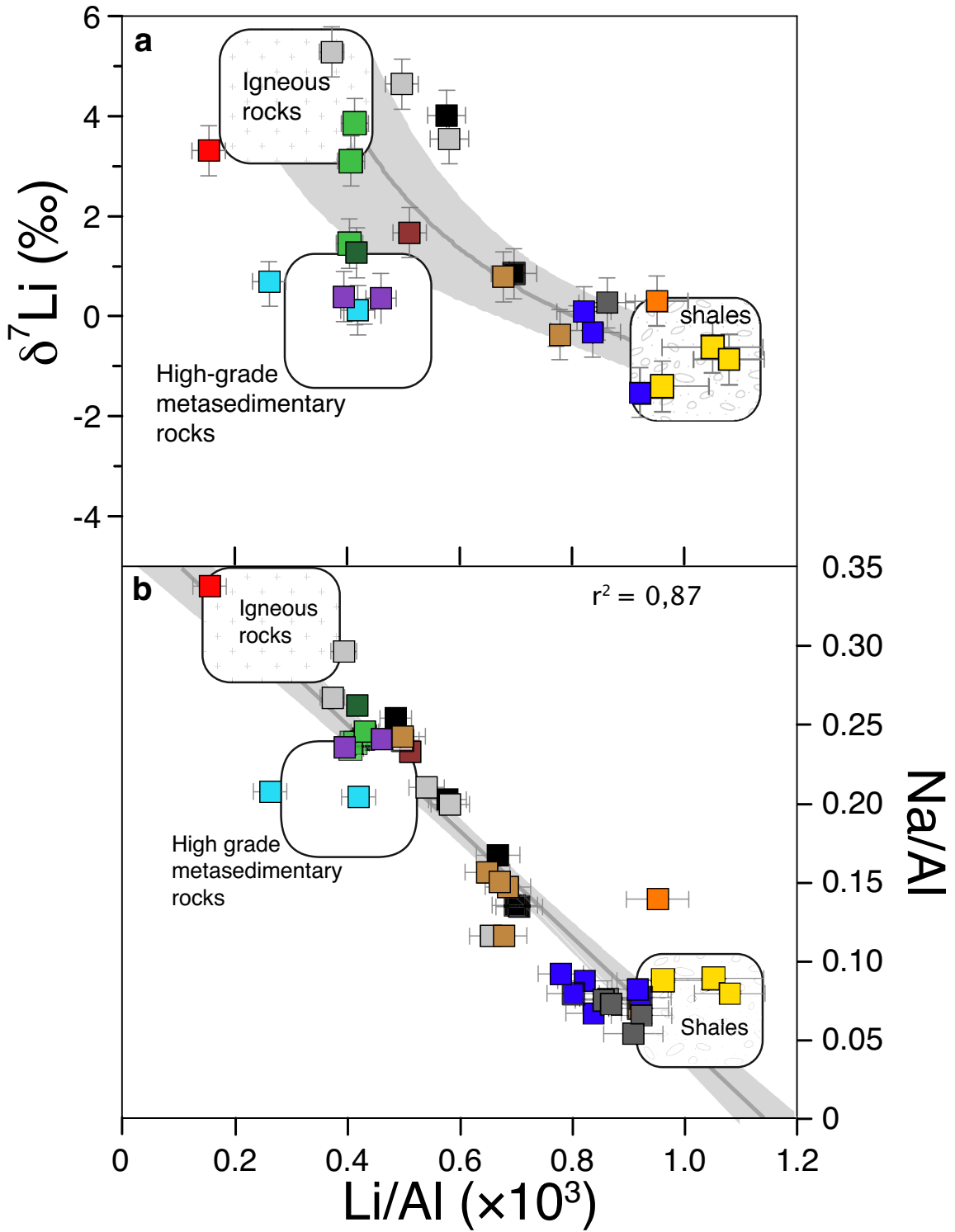


Figure 4

985
986

987

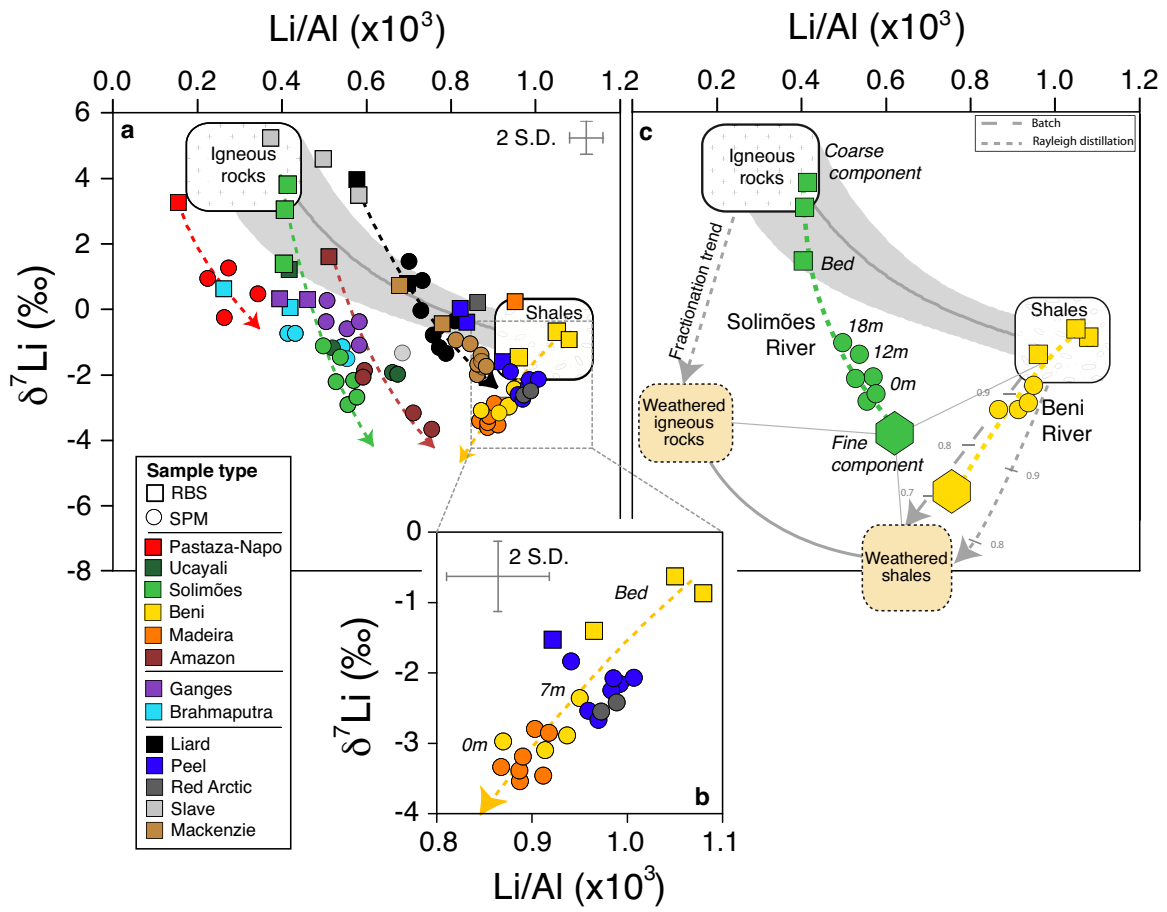


Figure 5

988

989

990

991

992

993

994

995

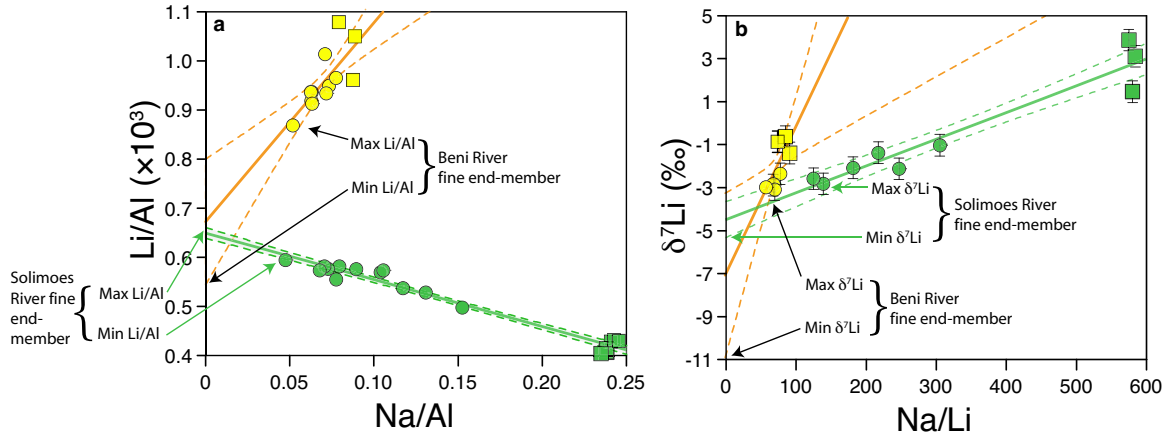


Figure 6

996
997

998

999

1000

1001

1002

1003

1004

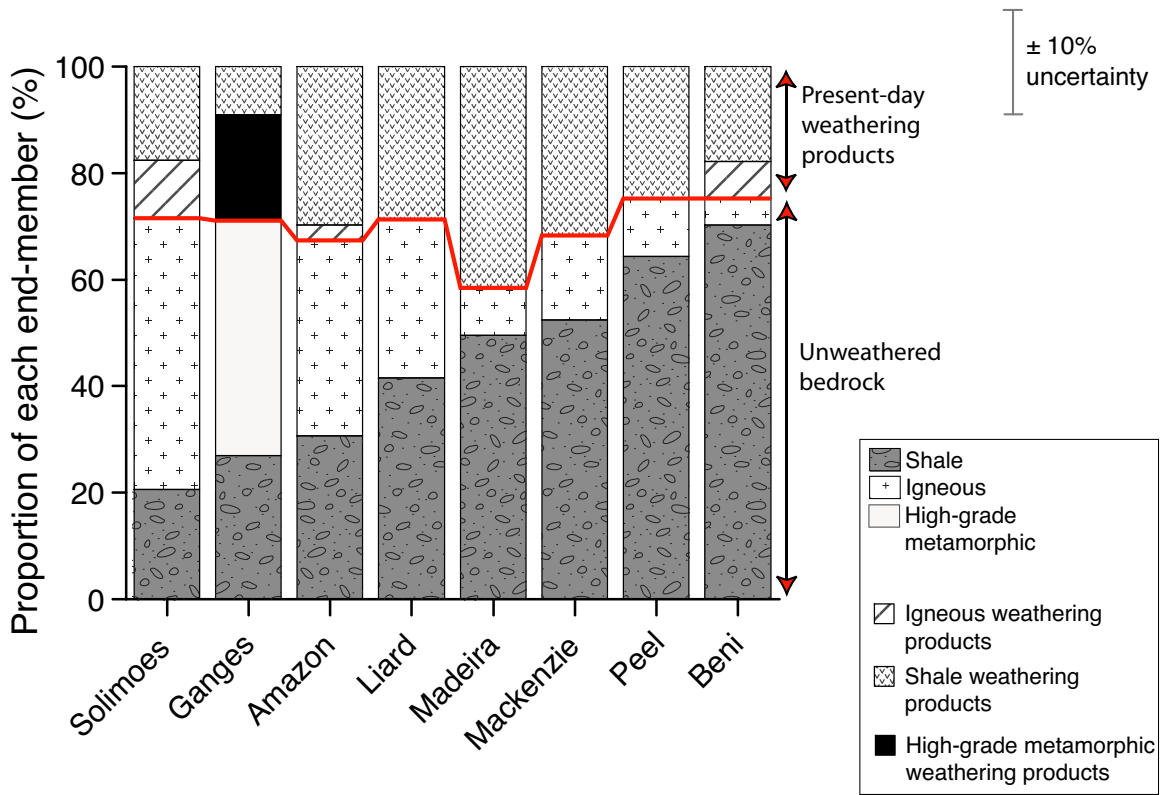


Figure 7

1005
 1006
 1007
 1008
 1009
 1010
 1011
 1012
 1013
 1014
 1015
 1016
 1017

1018 **Table captions**

1019 **Table 1:** Chemical and Li isotope data for the Mackenzie River system.

1020 **Table 2:** Chemical and Li isotope data for the Amazon River system. Numbers marked
1021 with an asterisk (*) are Li concentrations measured by ICP-AES at the Laboratory of
1022 “Géochimie des eaux” (IPGP, Paris)

1023 **Table 3:** Chemical and Li isotope data for the G-B River system. Numbers marked with
1024 an asterisk (*) are Li concentrations measured by ICP-AES at the Laboratory of
1025 “Géochimie des eaux” (IPGP, Paris)

1026

1027

1028

1029

1030

1031

1032

1033

1034

1035

1036

1037

1038 Table 1.

Sample	Date	River	Location	Type	Depth (m)	SPM (mg/L)	Al (ppm)	Li (ppm)	Na (ppm)	Si (ppm)	$\delta^7\text{Li}$ (‰)
CAN09_49	07/22/09	Red Arctic	Tsiigehtchic	Bed sands			43372	37	3294	297504	0,3
CAN09_50	07/22/09	Red Arctic	Tsiigehtchic	SPM	4	416	79837	78	2975	258931	-2,5
CAN09_51	07/22/09	Red Arctic	Tsiigehtchic	SPM	2	417	79022	78	3079	254831	-2,4
CAN09_52	07/22/09	Red Arctic	Tsiigehtchic	SPM	0	366	81849	80	2990	260974	
CAN09_53	07/22/09	Red Arctic	Tsiigehtchic	Bed sands			45330	42	2960	300177	
CAN10_17	09/07/10	Red Arctic	Tsiigehtchic	SPM	6	123	73830	71	3042	251246	
CAN10_18	09/07/10	Red Arctic	Tsiigehtchic	SPM	3	134	70602	69	3116	250826	
CAN10_19	09/07/10	Red Arctic	Tsiigehtchic	SPM	0	123	71608	70	3042	251246	
CAN10_20	09/07/10	Red Arctic	Tsiigehtchic	Bed sands			47146	40	3539	290371	
CAN10_21	09/07/10	Red Arctic	Tsiigehtchic	Bed sands			54010	47	3924	273590	
CAN09_01	07/15/09	Liard	Fort Simpson	SPM	6	462	47527	35	4985	309788	0,0
CAN09_02	07/15/09	Liard	Fort Simpson	SPM	4	191	63896	49	4125	272384	-1,1
CAN09_03	07/15/09	Liard	Fort Simpson	SPM	2	346	55730	42	4600	289898	-0,7
CAN09_04	07/15/09	Liard	Fort Simpson	SPM	0	166	64955	51	4266	273169	-1,3
CAN09_11	07/16/09	Liard	Fort Simpson	Bed sands			28744	17	5816	350604	4,0
CAN09_12	07/16/09	Liard	Fort Simpson	Bed sands			40620	28	5490	313359	0,9
CAN10_46	09/13/10	Liard	Fort Simpson	SPM	4,8	492	38265	27	5712	336460	1,5
CAN10_47	09/13/10	Liard	Fort Simpson	SPM	3	387	40858	30	5564	332907	0,9
CAN10_48	09/13/10	Liard	Fort Simpson	SPM	1,5	208	49220	40	4822	308928	-0,3
CAN10_49	09/13/10	Liard	Fort Simpson	SPM	0	79	73830	64	3709	262745	
CAN10_50	09/13/10	Liard	Fort Simpson	Bed sands			26796	13	6803	384839	
CAN10_51	09/14/10	Liard	Fort Simpson	Bed sands			32988	22	5512	338002	
CAN11_03	06/04/11	Liard	Fort Simpson	SPM	6,5	490	56524	43	5200	275974	
CAN11_04	06/04/11	Liard	Fort Simpson	SPM	5	595	52655	39	5304	282611	
CAN11_05	06/04/11	Liard	Fort Simpson	SPM	3,5	542	55058	42	5059	274805	
CAN11_06	06/04/11	Liard	Fort Simpson	SPM	1,5	495	57916	43	5141	271393	
CAN11_07	06/04/11	Liard	Fort Simpson	SPM	0	438	58509	45	5015	264288	
CAN11-62		Liard	Fort Simpson	Bed sands			41155	29	5519	299158	
CAN09_54	07/22/09	Mackenzie	Tsiigehtchic	Bed sands			40244	27	4659	304057	0,8
CAN09_43	07/22/09	Mackenzie	Tsiigehtchic	SPM	19,8	526	74757	65	3835	261520	
CAN09_44	07/22/09	Mackenzie	Tsiigehtchic	SPM	15	542	73873	64	3754	259239	-1,3
CAN09_45	07/22/09	Mackenzie	Tsiigehtchic	SPM	10	501	77953	68	3657	261362	-1,5
CAN09_46	07/22/09	Mackenzie	Tsiigehtchic	SPM	5	528	74407	65	3732	258730	-1,5
CAN09_47	07/22/09	Mackenzie	Tsiigehtchic	SPM	0	505	76477	67	3783	257323	-1,7
CAN09_48	07/22/09	Mackenzie	Tsiigehtchic	Bed sands			27225	14	5490	342499	
CAN10_08	09/07/10	Mackenzie	Tsiigehtchic	Bed sands			31326	21	4696	301589	
CAN10_10	09/07/10	Mackenzie	Tsiigehtchic	SPM	23	255	80393	72	3561	244655	
CAN10_11	09/07/10	Mackenzie	Tsiigehtchic	SPM	19,4	245	80658	69	3561	242599	
CAN10_12	09/07/10	Mackenzie	Tsiigehtchic	SPM	15	228	84468	73	3487	242552	
CAN10_13	09/07/10	Mackenzie	Tsiigehtchic	SPM	10	230	82934	72	3487	241383	
CAN10_14	09/07/10	Mackenzie	Tsiigehtchic	SPM	5	225	83304	72	3487	239140	
CAN10_15	09/07/10	Mackenzie	Tsiigehtchic	SPM	0	231	83833	72	3487	242552	
CAN10_16	09/07/10	Mackenzie	Tsiigehtchic	Bed sands			27913	14	6766	358803	
CAN11_65	06/11/11	Mackenzie	Tsiigehtchic	SPM	13	941	39509	27	5512	312667	

CAN11_66	06/11/11	Mackenzie	Tsiigehtchic	SPM	10	445	50607	39	5089	291446	
CAN11_67	06/11/11	Mackenzie	Tsiigehtchic	SPM	5	322	56614	46	4436	264428	
CAN11_68	06/11/11	Mackenzie	Tsiigehtchic	SPM	0	291	59948	49	4281	260268	
CAN10_22	09/08/10	Mackenzie	Inuvik	SPM	15		57334	45	4065	273174	
CAN10_23	09/08/10	Mackenzie	Inuvik	Bed sands			49321	38	4525	277002	-0,4
CAN10_26	09/08/10	Mackenzie	Inuvik	SPM	0	212	80870	70	3561	245076	
CAN10_27	09/08/10	Mackenzie	Inuvik	Bed sands			32290	22	4740	309115	
CAN10_28	09/09/10	Mackenzie	Inuvik	SPM	19	513	56947	46	4229	276161	-0,9
CAN10_29	09/09/10	Mackenzie	Inuvik	SPM	17	275	77165	67	3635	250498	-1,9
CAN10_30	09/09/10	Mackenzie	Inuvik	SPM	12	260	79864	68	3561	248301	
CAN10_31	09/09/10	Mackenzie	Inuvik	SPM	6	251	79441	70	3561	246665	
CAN10_32	09/09/10	Mackenzie	Inuvik	SPM	0	162	90608	79	3264	238298	-1,7
CAN10_34	09/09/10	Mackenzie	Inuvik	SPM	8	345	69014	58	3783	256295	
CAN10_35	09/09/10	Mackenzie	Inuvik	SPM	6	393	67427	57	3858	259333	-1,0
CAN10_36	09/09/10	Mackenzie	Inuvik	SPM	3	334	71502	61	3783	257136	
CAN10_37	09/09/10	Mackenzie	Inuvik	SPM	0	217	84363	73	3635	244095	-1,6
CAN10_38	09/09/10	Mackenzie	Inuvik	Bed sands			32258	21	5037	326363	
CAN09_31	07/18/09	Peace	Peace_Point	SPM		1515	81309	59	3160	265400	
CAN09_32	07/18/09	Peace	Peace_Point	Bed sands			51946	34	6009	323339	
CAN09_33	07/18/09	Peace	Peace_Point	Bed sands			34708	20	6914	345411	3,5
CAN09_28	07/18/09	Slave	Fort_Smith	SPM		125	77069	53	4251	275099	-1,3
CAN09_30	07/18/09	Slave	Fort_Smith	Bed sands			32739	12	8739	358831	
CAN10_65	09/15/10	Slave	Fort Smith	SPM			77271	60	4748	273356	
CAN10_66	09/15/10	Slave	Fort Smith	Bed sands			33168	17	7960	373060	4,1
CAN09_37	07/21/09	Peel	Fort McPherson	SPM	9	164	71094	71	3457	283326	-2,2
CAN09_38	07/21/09	Peel	Fort McPherson	SPM	6	150	72364	71	3398	283574	-2,2
CAN09_39	07/21/09	Peel	Fort McPherson	SPM	3	154	72285	71	3286	282261	-2,1
CAN09_40	07/21/09	Peel	Fort McPherson	SPM	0	113	80981	82	3331	273819	-2,1
CAN09_41	07/21/09	Peel	Fort McPherson	Bed sands			40620	34	2708	342723	-0,3
CAN09_42	07/22/09	Peel	Fort McPherson	Bed sands			52983	49	4065	301411	-1,5
CAN10_01	09/06/10	Peel	Fort McPherson	Bed sands			59647	55	4896	306684	
CAN10_03	09/07/10	Peel	Fort McPherson	SPM	8,5	250	58694	55	3338	305188	-1,8
CAN10_04	09/07/10	Peel	Fort McPherson	SPM	5,5	121	72401	69	3635	283312	-2,5
CAN10_05	09/07/10	Peel	Fort McPherson	SPM	2,5	105	75842	74	3561	279059	-2,7
CAN10_06	09/07/10	Peel	Fort McPherson	SPM	0	101	76053	73	3487	277376	
CAN10_07	09/07/10	Peel	Fort McPherson	Bed sands			34205	28	2982	360439	0,1
CAN11_77	06/11/11	Peel	Fort McPherson	SPM	6	325	58519	55	3680	285790	
CAN11_78	06/11/11	Peel	Fort McPherson	SPM	3	294	59964	57	3776	285556	
CAN11_79	06/11/11	Peel	Fort McPherson	SPM	0	146	72153	69	4028	267139	

1039

1040

1041

1042

1043 Table 2.

Sample	Date	River	Location	Type	Depth (m)	SPM (mg/L)	Al (ppm)	Li (ppm)	Na (ppm)	Si (ppm)	$\delta^7\text{Li}$ (‰)
AM05-15	06/06/05	Madeira	Foz Madeira	SPM	23	94	103611	90*	5312	271259	-3,33
AM05-17	06/06/05	Madeira	Foz Madeira	SPM	12	74	106544	94*	4956	263317	-3,53
AM05-18	06/06/05	Madeira	Foz Madeira	SPM	8	61	110435	101*	5090	252910	-3,45
AM05-19	06/06/05	Madeira	Foz Madeira	SPM	3	49	111822	99*	5194	245341	-3,38
AM05-20	06/06/05	Madeira	Foz Madeira	SPM	28		35756	34*	4971	395817	0,30
AM05-24	06/06/05	Madeira	Foz Madeira	SPM	21		73191	67*	5105	321001	-2,85
AM06-33	03/19/06	Madeira	Foz Madeira	SPM	12	1269	72339	65	5513	326125	
AM06-34	03/19/06	Madeira	Foz Madeira	SPM	6	524	86554	77	5646	300939	-3,18
AM06-35	03/19/06	Madeira	Foz Madeira	SPM	0	219	105221	91	5312	266672	
AM06-36	03/19/06	Madeira	Foz Madeira	SPM	15	455	85336	77	5483	300295	-2,79
AM06-37	03/19/06	Madeira	Foz Madeira	SPM	10	473	85590		5468	300328	-2,73
AM06-39	03/19/06	Madeira	Foz Madeira	SPM	11	461	88597		5438	296842	-2,82
AM06-43	03/19/06	Madeira	Foz Madeira	SPM	0	303	100324		5453	280915	-2,90
AM06-44	03/19/06	Madeira	Foz Madeira	Bed sands			25094		2723	403643	0,69
AM05-4	06/04/05	Solimoes	Manacapuru	SPM	28	283	69358		10387	319256	-0,51
AM05-6	06/04/05	Solimoes	Manacapuru	SPM	14	136	84081	45*	9860	290607	-1,39
AM06-1	03/15/06	Solimoes	Manacapuru	Bed sands			25698	11	6188	411180	
AM06-2	03/15/06	Solimoes	Manacapuru	Bed sands			36842	15	8777	391216	3,10
AM06-3	03/15/06	Solimoes	Manacapuru	Bed sands			31426	13	7486	401534	3,85
AM06-4	03/15/06	Solimoes	Manacapuru	Bed sands			25481	11	6180	405258	
AM06-5	03/15/06	Solimoes	Manacapuru	Bed sands			47017	19	11040	361844	1,45
AM06-6	03/15/06	Solimoes	Manacapuru	Bed sands			32538	14	7983	399317	
AM06-7	03/16/06	Solimoes	Manacapuru	SPM	20	425	70306	35	10714	319079	-1,04
AM06-9	03/16/06	Solimoes	Manacapuru	SPM	0	131	98042	57	7783	264077	
AM06-10	03/16/06	Solimoes	Manacapuru	SPM	22	302	86019	49	8925	280224	-2,09
AM06-11	03/16/06	Solimoes	Manacapuru	SPM	15	277	88745		8762	279417	-2,50
AM06-12	03/16/06	Solimoes	Manacapuru	SPM	10	209	87231	50	9207	283710	
AM06-13	03/16/06	Solimoes	Manacapuru	SPM	5	141	97613	54	7568	264213	-2,83
AM06-14	03/16/06	Solimoes	Manacapuru	SPM	0	79	100535	58	7301	260358	-2,60
AM06-15	03/16/06	Solimoes	Manacapuru	SPM	25	333	79539	42	10402	298769	-2,14
AM06-16	03/16/06	Solimoes	Manacapuru	SPM	18	143	90349	52	8080	275627	
AM06-17	03/16/06	Solimoes	Manacapuru	SPM	12	92	98074	57	6915	262999	
AM06-18	03/16/06	Solimoes	Manacapuru	SPM	6	73	99450	57	6729	260993	
AM06-19	03/16/06	Solimoes	Manacapuru	SPM	0	54	105972	63	5023	242023	
AM06-55	03/22/06	Amazonas	Obidos	SPM	55	341	69395	48	7427	324567	
AM06-58	03/22/06	Amazonas	Obidos	SPM	10	124	92652	68	6707	279930	
AM06-60	03/23/06	Amazonas	Obidos	SPM	35	482	84939	60	7523	291335	
AM06-63	03/23/06	Amazonas	Obidos	SPM	45	250	90032	64	7167	285591	-3,09
AM06-64	03/23/06	Amazonas	Obidos	SPM	20	141	98688		6395	271325	-2,99
AM06-65	03/23/06	Amazonas	Obidos	SPM	0	81	107370	81	5483	253531	-3,58
AM05-35	06/08/05	Amazonas	Obidos	SPM	58	318	65234		8354	332229	
AM05-36	06/08/05	Amazonas	Obidos	SPM	45	297	67961	40*	8577	325313	-1,79

AM05-37	06/08/05	Amazonas	Obidos	SPM	30	175	75907		8332	312522	-2,11
AM05-44	06/09/05	Amazonas	Obidos	SPM	42		29234		5646	359973	1,94
AM05-46	06/09/05	Amazonas	Obidos	SPM	51		29531	15*	6870	403312	1,67
AM07-1	05/05/07	Beni	Rurrenabaque	SPM	4,5	666	58225	59	4125	349421	
AM07-2	05/05/07	Beni	Rurrenabaque	SPM	3	236	91466	84	5743	298027	
AM07-3	05/05/07	Beni	Rurrenabaque	SPM	1,5	222	92928	87	5809	289123	
AM07-4	05/05/07	Beni	Rurrenabaque	SPM	0	109	95289	87	6025	289193	-3,09
AM07-5	05/05/07	Beni	Rurrenabaque	Bed sands			37991	41	3005	391375	-0,86
AM01-14	02/18/01	Beni	Rurrenabaque	Bed sands			67655	65*	5920		-1,39
AM07-6	05/07/07	Beni	Riberalta	SPM	7	2551	68469	65	5023	335487	-2,35
AM07-7	05/07/07	Beni	Riberalta	SPM	5	3373	64212	62	4971	341768	
AM07-8	05/07/07	Beni	Riberalta	SPM	2,5	2213	72805	68	5208	322919	
AM07-9	05/07/07	Beni	Riberalta	SPM	0	1003	83319	78	5231	302321	-2,88
AM07-10	05/07/07	Beni	Riberalta	Bed sands			35248	37	3124	394053	-0,62
AM01-16	02/21/01	Beni	Riberalta	SPM	0	1036	107113	93*	5550	273587	-2,99
AM08-10	04/25/08	Ucayali	Jenaro Herrera	SPM	23	641	84229	54*	10120	288269	-1,85
AM08-13	04/25/08	Ucayali	Jenaro Herrera	SPM	0	490	85664	58*	9964	278353	-1,90
AM08-14	04/25/08	Ucayali	Jenaro Herrera	Bed sands			48182	20*	12620	385261	1,27
AM08-17	04/25/08	Ucayali	Jenaro Herrera	SPM	23	2065	63805	33*	12902	340102	-1,02
AM08-36	05/04/08	Pastaza	Mouth	SPM	0	102	97031	26*	15840	246652	-0,18
AM08-37	05/04/08	Pastaza	Mouth	Bed sands			79814	12*	26955	291835	3,31
Napo 3		Napo		Bed sands < 125µm			80349	18*	22052		1,01
Napo 4		Napo		Bed sands < 125µm			78077	21*	19235		1,32
Coca 1		Napo		Bed sands < 125µm			78875	27*	14584		0,54

1044

1045 Table 3.

Sample	Date	River	Location	Type	Depth (m)	SPM (mg/L)	Al (ppm)	Li (ppm)	Na (ppm)	Si (ppm)	$\delta^7\text{Li}$ (‰)
BR8218	09/01/08	Ganga	Harding bridge	SPM	2	1390	73670	41*	8140	292340	-0,52
BR8217	09/02/08	Ganga	Harding bridge	SPM	4	1590	69430	40*	8140	298920	-0,31
BR8216	09/03/08	Ganga	Harding bridge	SPM	7	1590	69430	35*	8880	299390	-0,31
BR8215	09/04/08	Ganga	Harding bridge	SPM	12	3300	55120	28*	9620	332760	0,34
BR8221	09/05/08	Ganga	Harding bridge	Bed sands			46110	21*	11100	369420	0,36
IND99-19 S		Ganga	Harding bridge	Bed sands			47145	19*	11093		0,39
IND99-19 MES		Ganga	Harding bridge	SPM			94322	55*	4748	233473	-1,02
BR8210	08/31/08	Brahmaputra	Jamuna bg.	SPM	0	1000	86920	47*	11840	282940	-1,38
BR8211	08/31/08	Brahmaputra	Jamuna bg.	SPM	2,5	1400	77380	32*	13320	300330	-0,67
BR8208	08/31/08	Brahmaputra	Jamuna bg.	SPM	5	1700	74200	40*	13320	309730	-1,07
BR8207	08/31/08	Brahmaputra	Jamuna bg.	SPM	10	3600	65190	28*	14060	337930	-0,66
BR8213	08/31/08	Brahmaputra	Jamuna bg.	Bed sands	10		53530	14*	11100	312550	0,69
IND99-20 S		Brahmaputra	Jamuna bg.	Bed sands			72063	30*	14707		0,12

1046

1047